Peripheral serotonergic neurons regulate anxiety-like behavior and intestinal barrier immunity

Hailong Zhang[1,2,3], Yuko Hasegawa[1,2,3], Deborah R. Leitner[1,2,3], Ting Zhang[1,2,3], Masataka Suzuki[1,2,3], Ruaidhrí P. Jackson[4], Matthew K. Waldor[1,2,3]*

Affiliations:

[1]Division of Infectious Diseases, Brigham and Women's Hospital, Boston, MA 02115, USA

[2]Department of Microbiology, Harvard Medical School, Boston, MA 02115, USA

[3]Howard Hughes Medical Institute, Boston, MA 02115, USA

[4]Department of Immunology, Harvard Medical School, Boston, MA 02115, USA

*Corresponding author. Email: mwaldor@research.bwh.harvard.edu

Abstract:

Serotonergic circuits in the central nervous system play important roles in regulating mood and behavior, yet the functions of peripheral serotonergic neurons (PSN) are less understood. Here, we engineered mice lacking the serotonin-producing enzyme *Tph2* in peripheral neurons but with intact *Tph2* in central neurons. We discovered that PSN contribute to gut motility and are important in the control of anxiety-like behavior. These animals also had reduced abundance of serotonin receptor 7 (*Htr7*)-positive dendritic cells (DC) and IgA^+ B cells in the small intestine and elevated susceptibility to oral *Salmonella* infection. Mechanistic studies suggest that PSN-derived serotonin promotes gut homing/retention and activation of DC through *Htr7*, thereby facilitating DC-mediated differentiation of IgA^+ B cells from IgD^+ precursors. Bioinformatic analyses of our single-cell RNA-seq data uncovered novel patterns of bidirectional communication between specific subsets of enteric neurons and DC. Our findings underscore the interplay between enteric neurons and innate immune defense.

Keywords:

peripheral serotoninergic neurons, behavior, enteric nervous system, gut motility, neuro-immune axis, dendritic cell, IgA B cell, *Salmonella* infection, mucosal defense

In brief:

Peripheral serotonergic circuits are hubs for control of specific behaviors, gut motility and innate immune defense.

Highlights:

Peripheral serotonergic circuits control specific aspects of behavior.

Peripheral serotonergic neurons regulate gut motility, immunity and host defense.

Enteric serotonergic neurons remodel dendritic cell function to facilitate IgA B cell differentiation.

Bidirectional communication between enteric neurons and innate immune cells.

Main:

Communication between the gut and the brain, also known as the "gut-brain axis", is bidirectional [1]. Both the central (CNS) and peripheral nervous systems (PNS) are important for the proper maintenance of gastrointestinal homeostasis, and the gut in return influences multiple nervous system functions, including higher cognition and behavior [2, 3]. The CNS is derived from the neural tube, while the PNS, which includes the dorsal root ganglia, and autonomic and enteric nervous systems (ENS), arises from embryonic neural crest cells [4]. Only a small subset of neurons in the CNS and PNS produce 5-hydroxytryptamine (5-HT), the neurotransmitter commonly known as serotonin [5, 6] and most serotonin in the body is not generated by neurons but by intestinal enterochromaffin cells [7]. Although serotonergic neurons in the CNS have been the focus of much research, few studies have investigated the functions of peripheral serotonergic neurons. Single-cell RNA-seq analyses have shown that serotonergic neurons represent ~1% of sympathetic and enteric neurons (Furlan et al., 2016; May-Zhang et al., 2020).

Neuronal serotonin production relies on the enzyme tryptophan hydroxylase 2 (*Tph2*) [8]. In contrast, non-neuronal serotonin is generated by *Tph1* [9]. Studies with knock-out mice indicate that *Tph1* accounts for most of the serotonin found in blood and the gut [10] and plays important roles in diverse processes, including hemostasis, vascular tone, and immune modulation [11, 12]. In contrast, mice lacking *Tph2* exhibit several behavioral disorders, including decreased anxiety-like behavior and increased territorial aggression and reduced gut motility [13, 14].

Neuronal and non-neuronal serotonin both act through multiple serotonin receptors (Htr). Most research has focused on CNS serotonin receptors and a variety of psychiatric disorders are thought to be related to central serotonergic pathways [15]. The expression and functions of serotonin receptors in the intestine are less understood, although these receptors could be

valuable targets for drugs that selectively manipulate gut function without affecting the brain. The ENS is thought to regulate several aspects of GI physiology including intestinal motility, intestinal epithelial cell function, and nutrient absorption [16, 17]. Since the GI tract is home to the largest immune organ in the body, elucidating the interplay between enteric neurons and the innate immune system is critical for understanding the neuro-immune axis. However, contributions of particular subsets of enteric neurons to physiology and behavior have been difficult to assess in the absence of conditional knockout (KO) animals deficient in neuronal subsets.

Here, we studied the function of enteric serotonergic neurons by creating a conditional KO mouse model (*Tph2*$^{fl/fl}$*; Hand2-Cre*) lacking *Tph2* in peripheral neurons. The behavioral patterns of these mice were distinct from those of whole-body *Tph2* KO mice, linking peripheral serotonergic neurons to social behaviors. Moreover, our findings revealed that enteric serotonergic neurons support the gut homing/retention and activation of *Htr7* positive dendritic cells (DC) and IgA B cells in the small intestine and intestinal barrier defense against *Salmonella*. Bioinformatic analyses of single-cell RNA-seq data from enteric neurons and lamina propria DC suggests that there is robust bidirectional communication between specific subsets of enteric neurons and innate immune cells. Collectively, our findings highlight the key role of enteric neurons in controlling behavior, intestinal physiology, innate immune development and host defense.

Results:

Detection and deletion of serotonin synthesis gene *Tph2* in enteric neurons

In the CNS, serotonergic neurons originate in the brainstem and ramify throughout the brain, regulating a variety of brain functions and behaviors through a set of serotonin receptors [18, 19]. The production and function of serotonin by neurons in the peripheral nervous system (PNS) has received relatively little attention. To quantify the enteric serotonergic neuronal population, we used FACS to sort cells bearing the neuronal marker *Uchl1* [20] from the small intestines of infant mice and then carried out single-nucleus RNA-seq. These analyses revealed that a small proportion (~2%) of cells expressed *Tph2* as well as *Ret*, an established marker of enteric neurons [21], indicating the presence of enteric serotonergic neurons (Figures 1A and S1A-S1C). *Tph2* transcripts were observed in various subtypes of enteric neurons (Figure 1A). *Tph2* transcripts were also present in sorted enteric neurons from the small intestines of adult mice but not in the intestinal epithelium or lamina propria immune cells (Figure 1B). In contrast, *Tph1* transcripts were detected in the latter two small intestinal cell populations but not in enteric neurons (Figure 1B).

Given the lack of a promoter specific for enteric neurons, to investigate the functions of enteric serotonergic neurons, we generated a conditional knockout mouse (*Tph2*$^{fl/fl}$*; Hand2-Cre*), leveraging the *Hand2* promoter (Figure 1B), which is active in neural crest-derived cells including enteric neurons and other neurons in the PNS [17, 22, 23], but not in the brain [5]. We confirmed that *Tph2* transcripts were absent in the gut but preserved in the brain in *Tph2*$^{fl/fl}$*; Hand2-Cre* mice (Figure 1C), establishing that these animals are deficient in expression of serotonin synthesis gene *Tph2*, at least in the ENS. The network of neuronal fibers in the myenteric plexus in *Tph2*$^{fl/fl}$ and *Tph2*$^{fl/fl}$*; Hand2-Cre* mice appeared similar (Figure S1D), and

comparable neuronal gene expression patterns were found in *Tph2*$^{fl/fl}$ and *Tph2*$^{fl/fl}$*; Hand2-Cre* mice (Figure S1E). Together, these results suggest that serotonin produced by peripheral neurons are not essential for the formation of the myenteric plexus and are consistent with studies of *Tph2*$^{-/-}$ mice that showed the absence of *Tph2*-expressing neurons in the brain does not grossly influence brain development [24, 25].

PSN influence specific aspects of behavior

Our conditional KO mice enabled us to separate the function of serotonergic neurons in the CNS and PNS in the context of behavioral disorders. Thus, we compared behaviors of *Tph2*$^{fl/fl}$ and *Tph2*$^{fl/fl}$*; Hand2-Cre* mice to investigate whether PSN contribute to any of the behavioral disorders that have been observed in the whole-body *Tph2* KO mice [14, 26]. The absence of neuronal serotonin production in mice and rats lacking the *Tph2* gene is associated with heightened territorial aggression, measured in resident-intruder assays [27], as well as decreased anxiety-like behavior, measured in elevated plus and elevated zero maze tests [28]. In these experiments, we first examined WT and *Tph2*$^{-/-}$ mice to replicate reported behavioral defects of the whole-body knockout (Figures 2A-2D and movie S1). Co-housed littermates were used for these comparisons in order to control for potential microbiota-related effects.

As observed in whole-body *Tph2* KO animals [14], the deficiency of *Tph2* activity in the PNS did not impact overall locomotor activity (Figure 2A), suggesting that serotonergic neurons in either the central or peripheral have little influence on general movement. In contrast to the *Tph2*$^{-/-}$ animals, the *Tph2*$^{fl/fl}$*; Hand2-Cre* mice did not exhibit heightened territorial aggression (Figure 2B and movie S2), consistent with the finding that aggression originates from a subset of *Tph2* neurons in the brain [29]. Notably, the conditional *Tph2* KO mice displayed similar increased exploration in the open arm of the elevated plus and zero maze as observed in the whole-body *Tph2* KO animals (Figures 2C and 2D), suggesting that *Tph2* activity in peripheral neurons plays an important role in inhibiting anxiety-like behaviors. Together, these observations reveal that PSN control important and specific aspects of behavior.

PSN control gut motility and abundance of intestinal dendritic and IgA B cells

Whole-body *Tph2* KO animals have reduced gut motility [13] but the contribution of PSN to intestinal transit has been difficult to assess because a *Tph2* knockout specific to peripheral neurons has not been available. Two independent assays revealed that the *Tph2*$^{fl/fl}$*; Hand2-Cre* mice had a gut motility defect compared to co-housed *Tph2*$^{fl/fl}$ littermates (Figures 3A and S2A), demonstrating that PSN contribute to intestinal motility. Although the *Tph2*$^{fl/fl}$*; Hand2-Cre* mice had a gut motility defect, the overall architecture of the small intestine and colon appeared to be intact in these animals (Figure S2B).

To explore the possibility that serotonergic circuits modify epithelial cell function, we analyzed the gene expression profiles of epithelial cells isolated from the small and large intestines of WT and *Tph2*$^{-/-}$ mice. The serotonin receptor 4 (*Htr4*) was the dominant serotonin receptor expressed in small intestinal epithelial cells in our bulk RNA-seq analyses (Figure S2C) and in re-analysis of small intestinal epithelial single-cell RNA-seq from Tsang et al [30] (Figure S2D). However, the transcriptomes of co-housed littermates of WT and *Tph2*$^{-/-}$ mice were similar (Figures S2E and S2F), suggesting that neuronal *Tph2*-derived serotonin does not impact epithelial cell function and that the 5-HT_4 receptor on small intestinal epithelial cells could be mainly responsive to non-neuronal *Tph1*-derived serotonin. The microbiota in these animals was also similar (Figures S2G and S2H). In contrast, when the littermate WT and the *Tph2*$^{-/-}$ mice were not co-housed, but raised separately according to their genotypes, there were substantial differences in the gene expression profiles observed in their intestinal epithelia (Figures S2I and S2J), potentially explaining the previously reported differences in epithelial gene expression in these animals [31].

We also compared the gene expression profiles of lamina propria derived immune cells ($CD45^+$) in co-housed littermate WT and *Tph2*$^{-/-}$ mice to address whether serotonergic neurons

modulate intestinal immune cell function. In $CD45^+$ cells derived from the small intestines of *Tph2*$^{-/-}$ mice there was less expression of genes linked to B cell activation and dendritic cell differentiation than in WT animals (Figures 3B and S3A). In contrast, the gene expression profiles of $CD45^+$ cells isolated from the colons of *Tph2*$^{-/-}$ and WT mice were similar (Figure S3B). FACS-based immune profiling of $CD45^+$ cells (Figure S3C) isolated from the lamina propria of the small intestines from *Tph2*$^{-/-}$ and *Tph2*$^{fl/fl}$*; Hand2-Cre* mice also revealed that PSN modify immune cell composition in the small intestine. Both whole-body and conditional KO animals had reduced lamina propria DCs (LPDC) compared to the respective littermate controls (Figure 3C). Even though the total fraction of B and T cells were similar in KO and control animals (Figures 3D and S3D), there were increased IgD^+ B cells and decreased IgA^+ B cells in both the whole-body and conditional KO animals (Figure 3D), consistent with a defect in the differentiation of IgD^+ to IgA^+ B cells. A reduction of fecal IgA (Figure 3E) and small intestinal IgA^+ B cells was also observed in the *Tph2*$^{fl/fl}$*; Hand2-Cre* mice (Figures 3F and S3E). The reduced abundance of IgA^+ B cells seemed to be restricted to the small intestinal lamina propria, as the number of IgA^+ B cells was similar in Peyer's Patches (PP) and mesenteric lymph nodes (MLN) from *Tph2*$^{fl/fl}$ and *Tph2*$^{fl/fl}$*; Hand2-Cre* mice (Figure S3F). These data suggest that *Tph2* activity, and presumably serotonin production, in PSN promotes the development of IgA^+ B cells from IgD^+ precursors in the lamina propria of the small intestine.

Serotonin remodels lamina propria DC function

We hypothesized that the reduced abundance of LPDCs in the absence of serotonin production by peripheral serotonergic neurons contributes to the defect in B cell differentiation from IgD^+ precursor to IgA^+ B cells. To begin to assess whether serotonin modulates LPDC function, initially we analyzed the gene expression profiles of sorted LPDCs and found that *Htr7* is the predominant serotonin receptor expressed in these cells (Figure 4A). Re-analyses of single-cell RNA-seq data of small intestinal lamina propria immune cells [32] revealed that *Htr7* expression is primarily restricted to LPDCs (Figure 4B), suggesting that this G-protein coupled receptor enables LPDCs to respond to serotonin. To further characterize the effect of serotonin on LPDCs, we treated FACS-isolated LPDCs [33] in tissue culture with either serotonin (5-HT) or a combination of serotonin and the serotonin receptor *Htr7* antagonist SB269970 and analyzed their gene expression profiles. The abundance of 160 transcripts was increased >2-fold (adjusted p-value $<10^{-5}$) in a *Htr7*-dependent manner (Figure 4C). Many of the serotonin-induced, *Htr7*-dependent pathways were associated with immune regulation (Figure 4D). Consistent with our findings of reduced B-cell maturation and LPDC abundance in the *Tph2*$^{fl/fl}$*; Hand2-Cre* mice, these genes/pathways included loci linked to DC activation, such as *Cd83* [34], Figures 4C and S4A), integrin signaling (Figure 4D), which is associated with immune cell adhesion [35], as well as genes linked to DC-mediated activation/differentiation of B cells. The latter set of genes included *Cd40* [36], *Il6* [37] and *Lrrc32* (Figure S4B), a protein that promotes TGF-β activity [38, 39] that is linked to stimulation of IgA class switching [40].

We used co-culture experiments to test the hypothesis that serotonin-treated LPDC can promote the differentiation of IgD^+ B cells to IgA-secreting cells. Co-culture of IgD^+ B cells with LPDC triggered IgA production as described [37]; furthermore, the addition of serotonin augmented the abundance of IgA measured in supernatants (Figure 4E). Serotonin stimulation of

LPDC mediated IgA production was ablated by an *Htr7* antagonist, demonstrating that the effect of this neurotransmitter relies on *Htr7* dependent signaling pathways. Together, these observations suggest that serotonin remodels DC function to promote IgA class switching.

PSN remodel lamina propria DC function

We hypothesized that *in vivo*, PSN-derived serotonin remodels LPDC function in a *Htr7* dependent manner. To test this idea, LPDC from *Tph2*$^{fl/fl}$ and *Tph2*$^{fl/fl}$*; Hand2-Cre* mice were isolated by positive selection for single-cell RNA-seq (Figure S5A). Among MHCII+ cells, there was a lower proportion of LPDC in the *Tph2*$^{fl/fl}$*; Hand2-Cre* mice vs WT controls (Figure S5B and S5C), as observed above by FACS-based analysis (Figure 3C). Seven clusters of Cd11c+ cells were identified (Figure 5A). The proportion of cells in clusters 0 and 4 was reduced in *Tph2*$^{fl/fl}$*; Hand2-Cre* mice vs *Tph2*$^{fl/fl}$ animals (35.6% to 19.7% and 8.4% to 5.4%, respectively) but not in clusters 2 and 5 (Figures 5A and 5B). Since all four of these clusters were found to express *Htr7* (Figure 5C), these findings suggest that PSN and this serotonin receptor play a role in the homing to and/or survival of specific DC subsets in the lamina propria of the small intestine.

Notably, only cluster 0 and 4 LPDC, whose relative abundance was reduced in the absence of serotonin from PSN, expressed *Ccr7* (Figures 5C and 5D), a chemokine receptor that plays a critical role in cell-cell interaction (Hashizume-Takizawa et al., 2019; Jang et al., 2006). Thus, the reduced homing/retention of these two groups of LPDCs in the lamina propria may be attributable to reduced *Ccr7*expression (Figures 5D and 5E). Additional comparisons showed

that some of the most highly serotonin-induced genes in LPDC *in vitro* (Figure 4C) exhibited reduced expression in cluster 0 cells *in vivo* in *Tph2*$^{fl/fl}$*; Hand2-Cre* mice vs control animals; these genes included TGF-β activator *Lrrc32*, DC activation marker *Cd83*, *Dusp5* as well as *Ccr7* (Figure 5E). These observations are consistent with the idea that serotonin derived from PSN stimulates expression of genes linked to DC homing/retention and differentiation in certain subsets of LPDC, supporting the novel concept of functionally important interactions between PSN and LPDCs *in vivo*.

Given the reduced abundance of LPDC in the *Tph2*$^{fl/fl}$*; Hand2-Cre* mice, we used an *in vivo* DC homing assay (Figure 5F), to test the hypothesis that PSN promote DC homing/retention to the PP and MLN as well as to the small intestine lamina propria. No difference in the recruitment of labelled bone-marrow derived DC to the PP or MLN of *Tph2*$^{fl/fl}$ vs *Tph2*$^{fl/fl}$*; Hand2-Cre* mice (Figure S5D) was observed, indicating that the lymphoid tissue homing of DC is intact in the conditional KO mice. However, there was greater abundance of labelled DC in the lamina propria of *Tph2*$^{fl/fl}$ vs *Tph2*$^{fl/fl}$*; Hand2-Cre* mice (Figure 5G), suggesting the presence of PSN in the lamina propria may promote the retention of DC in this site. Furthermore, treatment of DC with an *Htr7* antagonist reduced their abundance in the lamina propria (Figure 5G), suggesting that serotonin signaling through *Htr7* on DC promotes the residency of these cells in the small intestine lamina propria. This mechanism could account for the reduced abundance of IgA^{+} B cells in mice deficient in *Tph2* in peripheral serotonergic neurons. Together, these observations suggest a new axis of interaction between PSN and the immune system: peripheral serotonergic neuron-derived serotonin promotes both retention and remodeling of DC function through *Htr7* signaling, thereby increasing the DC population in the small intestine that can induce IgA^{+} B cell development.

263

PSN protect against infection with an enteric pathogen

Finally, we sought to investigate the role of serotonergic neurons in defense against *Salmonella enterica serovar typhimurium*, a model enteric pathogen that disseminates from the intestine following oral inoculation. After oral infection with *Salmonella*, both whole body and PSN-specific *Tph2* KO mice had increased pathogen burdens in the spleen and liver (Figures 6A and 6B) and reduced survival compared with co-housed littermate controls (Figures 6C and 6D). Animals deficient in mucosal IgA also exhibit survival defects with *Salmonella* challenge [41], suggesting that the defect in the differentiation of IgD^+ B cells to IgA-secreting cells in PSN-specific *Tph2* KO mice increases susceptibility to this pathogen. In contrast, when the pathogen was administered intravenously to WT and *Tph2* KO mice, there was no difference in survival and both groups succumbed to infection with similar kinetics (Figure 6E). Together, these observations suggest that while systemic defenses are intact in animals deficient in *Tph2*, serotonin derived from peripheral neurons inhibits pathogen dissemination by augmenting the defense of intestinal barriers.

Bidirectional communication between enteric neurons and LPDC

Our understanding of how interactions between the ENS and the gut immune system contribute to intestinal homeostasis is limited. We used CellChat [42] to begin to infer and analyze the intercellular communication networks within the ENS-innate immune axis. For these analyses the scRNA-seq data from the 4,347 enteric neurons and 3,284 LPDCs sequenced in this study were utilized (Figures 7A and S6A). These analyses revealed that most of the significant cell-cell interaction pathways were between neuron subtypes and fewer interactions were predicted between neurons and DCs and DCs and DCs (Figure 7B). Furthermore, enteric neurons and LPDCs generally exhibit different patterns of communication that rely on distinct pathways (Figure 7C).

Among the ligand-receptor interactions between enteric neurons and DCs respectively inferred by these analyses (Figures 7D and 7G), we uncovered significant interactions driven by neuronal production of 'immune' ligands such as *Il7*, *Flt3l* and *Ccl25* and expressed DC receptors, *Il7R*, *Flt3*, and *Ccr9*, that are known to regulate DC function [43] (Figures 7D and 7E). Interactions between neuronal *Ptn*, a ligand linked to growth and cytokine regulation [44], and *Ncl* and *Sdc4* receptors on DCs was the most significant interaction detected (Figures 7E, 7F and S6B), suggesting that enteric neuron play a role in controlling activation/proliferation of LPDC. Notably, these analyses independently predicted the ENS-DC interaction through the serotonin-*Htr7* pathway (Figures 7D and 7E).

DC produced ligands, including several chemokines were predicted to interact with chemokine receptors, such as *Ackr1*, on enteric neurons (Figures 7G and 7H), suggesting that innate immune cells regulate ENS function. DCs also appear to control neuronal energy homeostasis, since the

Nampt/Visfatin-Insulin receptor pathway was the most significant interaction predicted (Figures 7H, 7I and S6C).

Finally, these analyses identified putative interactions between specific neuron and DC clusters. For example, *Il7* expression was restricted to enteric neuron cluster 4, while *Il7R* expression was exclusive to LPDC cluster 0 (Figures 7K and 7L), suggesting that cluster 4 neurons may control the proliferation of this DC subset [45]. Further investigation is necessary to validate this interaction and to elucidate its significance. However, this computational approach strongly suggests that there is a larger range of bidirectional cross talk between enteric neurons and innate immune cells than was appreciated.

Discussion:

Serotonin has long been known to control multiple biological processes in the host as well to influence the commensal microbiota and pathogens [46, 47]. Serotonin produced by *Tph1* in non-neuronal cells generally controls different activities than serotonin produced by *Tph2* in neurons [12, 48]. While the roles of CNS serotonergic neurons in cognition and behavior have been well-studied, here, we investigated the roles of peripheral neuron-derived serotonin by creating conditional KO mice that are deficient in *Tph2* in the PNS and not the CNS. Our findings demonstrate that serotonin produced by peripheral serotonergic neurons impacts diverse physiological processes, including behavior, gut motility, immune homeostasis and enteric defense. These diverse phenotypes are likely to be interrelated. For example, gut motility defects have been linked to defense against intestinal helminths [49] and macrophage and DC defects have been associated with reduced gut motility [50, 51]. Nevertheless, our findings suggest that peripheral serotonergic circuits in the intestine represent a new signaling hub for the control of specific behaviors and intestinal physiology and immune state in homeostasis and disease.

The overlapping and distinct behavioral patterns in whole-body and conditional *Tph2* KO animals suggest that, at least in part, serotonergic neurons in the PNS control specific aspects of behavior. Territorial aggression appears to be mediated by CNS serotonergic circuits, since the conditional KO animals did not exhibit elevated aggression. Surprisingly, the $Tph2^{-/-}$ and $Tph2^{fl/fl}$*; Hand2-Cre* animals both showed elevated exploratory behavior that is thought to reflect decreased anxiety-like behavior. The PNS is heterogeneous and small subsets of neural crest derivatives in the ENS as well as dorsal root ganglia and autonomic neurons express *Tph2* [52]. Dissecting the specific roles of serotonergic neurons in the PNS as well as potential interactions of peripheral and central serotonergic circuits in regulating anxiety-like behaviors is of interest.

Nevertheless, our observations raise the possibility that at least part of the action of anxiolytic medications that block serotonin reuptake (SSRIs) target serotonin signaling in the PNS. Defining the cellular networks and mechanisms through which peripheral serotonergic neurons regulate behavior may reveal new targets for pharmacological interventions for anxiety as well as disorders of gut motility.

Gene expression profiling uncovered the cell-type specificity of the expression of serotonin receptors. Enteric sensory neurons expressed *Htr3a* (Figures S6D and S6E), whereas *Htr4* was expressed in intestinal epithelial cells (Figure S2D), and *Htr7* in LPDC (Figures 4A and 4B). Thus, it may be possible to develop drugs that specifically bind these receptors, enabling precise targeting of specific cell types in the intestine. Engineering these compounds so that they are unable to penetrate the blood-brain barrier could prevent untoward central nervous system-related side effects.

Our findings illuminate a novel neuro-immune interaction [53, 54] in which serotonin, a neurotransmitter, controls LPDC function to promote IgA B cell differentiation. The 5-HT_7 receptor on LPDC appears to be critical for PSN to activate LPDCs, suggesting that serotonin derived from peripheral serotonergic neurons may account for some of the diverse immune phenotypes linked to *Htr7* [55] and raising the possibility that drugs that activate or inhibit this receptor may be useful as immunomodulatory agents. Additional studies are required to decipher whether signaling between PSN and LPDC is through a synapse-like mechanism, where there is a direct interaction between LPDCs and PSN, or via an indirect pathway that ultimately promotes DC retention and activation in the small intestinal lamina propria (Figure S5E).

Regardless of the precise mechanism through which PSN control LPDC, the absence of peripheral serotonergic neuron derived serotonin impaired mucosal defense against *Salmonella*.

Bioinformatic analyses using CellChat and similar pipelines [56] to systematically and quantitatively infer intercellular communication networks will be invaluable for deciphering neuro-immune interactions. The predicted interactions between enteric neurons and innate immune cells that we uncovered suggest that there is a complex bidirectional dialogue between specific subsets of enteric neurons and of DC. Functional analyses based on these inferences will reveal new insights into the roles of the ENS in innate immune regulation, as well as the potential remodeling of enteric neuronal function by innate immune cells.

References

1. Carabotti, M., Scirocco, A., Maselli, M.A. & Severi, C. The gut-brain axis: interactions between enteric microbiota, central and enteric nervous systems. *Ann Gastroenterol* **28**, 203-209 (2015).

2. Kunze, W.A. & Furness, J.B. The enteric nervous system and regulation of intestinal motility. *Annu Rev Physiol* **61**, 117-142 (1999).

3. Needham, B.D. *et al.* A gut-derived metabolite alters brain activity and anxiety behaviour in mice. *Nature* **602**, 647-653 (2022).

4. Sauka-Spengler, T. & Bronner-Fraser, M. A gene regulatory network orchestrates neural crest formation. *Nat Rev Mol Cell Biol* **9**, 557-568 (2008).

5. Okaty, B.W. *et al.* A single-cell transcriptomic and anatomic atlas of mouse dorsal raphe Pet1 neurons. *Elife* **9** (2020).

6. May-Zhang, A.A. *et al.* Combinatorial Transcriptional Profiling of Mouse and Human Enteric Neurons Identifies Shared and Disparate Subtypes In Situ. *Gastroenterology* (2020).

7. Erspamer, V. & Asero, B. Identification of enteramine, the specific hormone of the enterochromaffin cell system, as 5-hydroxytryptamine. *Nature* **169**, 800-801 (1952).

8. Walther, D.J. *et al.* Synthesis of serotonin by a second tryptophan hydroxylase isoform. *Science* **299**, 76 (2003).

9. Sze, J.Y., Victor, M., Loer, C., Shi, Y. & Ruvkun, G. Food and metabolic signalling defects in a Caenorhabditis elegans serotonin-synthesis mutant. *Nature* **403**, 560-564 (2000).

10. Brommage, R. *et al.* Adult Tph2 knockout mice without brain serotonin have moderately elevated spine trabecular bone but moderately low cortical bone thickness. *Bonekey Rep* **4**, 718 (2015).

11. Herr, N., Bode, C. & Duerschmied, D. The Effects of Serotonin in Immune Cells. *Front Cardiovasc Med* **4**, 48 (2017).

12. Amireault, P., Sibon, D. & Cote, F. Life without peripheral serotonin: insights from tryptophan hydroxylase 1 knockout mice reveal the existence of paracrine/autocrine serotonergic networks. *ACS Chem Neurosci* **4**, 64-71 (2013).

13. Li, Z. *et al.* Essential roles of enteric neuronal serotonin in gastrointestinal motility and the development/survival of enteric dopaminergic neurons. *J Neurosci* **31**, 8998-9009 (2011).

14. Mosienko, V. *et al.* Exaggerated aggression and decreased anxiety in mice deficient in

brain serotonin. *Transl Psychiatry* **2**, e122 (2012).

15. Mann, J.J. Role of the serotonergic system in the pathogenesis of major depression and suicidal behavior. *Neuropsychopharmacology* **21**, 99S-105S (1999).

16. Mourad, F.H. & Saade, N.E. Neural regulation of intestinal nutrient absorption. *Prog Neurobiol* **95**, 149-162 (2011).

17. Jarret, A. *et al.* Enteric Nervous System-Derived IL-18 Orchestrates Mucosal Barrier Immunity. *Cell* **180**, 813-814 (2020).

18. Hornung, J.P. The human raphe nuclei and the serotonergic system. *J Chem Neuroanat* **26**, 331-343 (2003).

19. Barnes, N.M. & Sharp, T. A review of central 5-HT receptors and their function. *Neuropharmacology* **38**, 1083-1152 (1999).

20. Osaka, H. *et al.* Ubiquitin carboxy-terminal hydrolase L1 binds to and stabilizes monoubiquitin in neuron. *Hum Mol Genet* **12**, 1945-1958 (2003).

21. Heanue, T.A. & Pachnis, V. Ret isoform function and marker gene expression in the enteric nervous system is conserved across diverse vertebrate species. *Mech Dev* **125**, 687-699 (2008).

22. Morikawa, Y. *et al*. The basic helix-loop-helix factor Hand 2 regulates autonomic nervous system development. *Dev Dyn* **234**, 613-621 (2005).

23. Hendershot, T.J. *et al.* Expression of Hand2 is sufficient for neurogenesis and cell type-specific gene expression in the enteric nervous system. *Dev Dyn* **236**, 93-105 (2007).

24. Gutknecht, L. *et al*. Deficiency of brain 5-HT synthesis but serotonergic neuron formation in Tph2 knockout mice. *J Neural Transm (Vienna)* **115**, 1127-1132 (2008).

25. Montalbano, A. *et al.* Cellular resilience: 5-HT neurons in Tph2(-/-) mice retain normal firing behavior despite the lack of brain 5-HT. *Eur Neuropsychopharmacol* **25**, 2022-2035 (2015).

26. Peeters, D.G.A. *et al.* Enhanced aggressive phenotype of Tph2 knockout rats is associated with diminished 5-HT(1A) receptor sensitivity. *Neuropharmacology* **153**, 134-141 (2019).

27. Koolhaas, J.M. *et al.* The resident-intruder paradigm: a standardized test for aggression, violence and social stress. *J Vis Exp*, e4367 (2013).

28. Walf, A.A. & Frye, C.A. The use of the elevated plus maze as an assay of anxiety-related behavior in rodents. *Nat Protoc* **2**, 322-328 (2007).

29. Niederkofler, V. *et al.* Identification of Serotonergic Neuronal Modules that Affect

Aggressive Behavior. *Cell Rep* **17**, 1934-1949 (2016).

30. Tsang, D.K.L. *et al*. A single cell survey of the microbial impacts on the mouse small intestinal epithelium. *Gut Microbes* **14**, 2108281 (2022).

31. Zhu, P. *et al.* Gut microbiota drives macrophage-dependent self-renewal of intestinal stem cells via niche enteric serotonergic neurons. *Cell Res* **32**, 555-569 (2022).

32. Xu, H. *et al.* Transcriptional Atlas of Intestinal Immune Cells Reveals that Neuropeptide alpha-CGRP Modulates Group 2 Innate Lymphoid Cell Responses. *Immunity* **51**, 696-708 e699 (2019).

33. Shi, G.P. *et al*. Cathepsin S required for normal MHC class II peptide loading and germinal center development. *Immunity* **10**, 197-206 (1999).

34. Lechmann, M., Berchtold, S., Hauber, J. & Steinkasserer, A. CD83 on dendritic cells: more than just a marker for maturation. *Trends Immunol* **23**, 273-275 (2002).

35. Luo, B.H., Carman, C.V. & Springer, T.A. Structural basis of integrin regulation and signaling. *Annu Rev Immunol* **25**, 619-647 (2007).

36. Fayette, J. *et al.* Human dendritic cells skew isotype switching of CD40-activated naive B cells towards IgA1 and IgA2. *J Exp Med* **185**, 1909-1918 (1997).

37. Mora, J.R. *et al.* Generation of gut-homing IgA-secreting B cells by intestinal dendritic cells. *Science* **314**, 1157-1160 (2006).

38. Dedobbeleer, O., Stockis, J., van der Woning, B., Coulie, P.G. & Lucas, S. Cutting Edge: Active TGF-beta1 Released from GARP/TGF-beta1 Complexes on the Surface of Stimulated Human B Lymphocytes Increases Class-Switch Recombination and Production of IgA. *J Immunol* **199**, 391-396 (2017).

39. Wang, R. *et al*. GARP regulates the bioavailability and activation of TGFbeta. *Mol Biol Cell* **23**, 1129-1139 (2012).

40. Reboldi, A. *et al*. IgA production requires B cell interaction with subepithelial dendritic cells in Peyer's patches. *Science* **352**, aaf4822 (2016).

41. Wijburg, O.L. *et al.* Innate secretory antibodies protect against natural Salmonella typhimurium infection. *J Exp Med* **203**, 21-26 (2006).

42. Jin, S. *et al.* Inference and analysis of cell-cell communication using CellChat. *Nat Commun* **12**, 1088 (2021).

43. Persson, E.K., Scott, C.L., Mowat, A.M. & Agace, W.W. Dendritic cell subsets in the intestinal lamina propria: ontogeny and function. *Eur J Immunol* **43**, 3098-3107 (2013).

44. Sorrelle, N., Dominguez, A.T.A. & Brekken, R.A. From top to bottom: midkine and

pleiotrophin as emerging players in immune regulation. *J Leukoc Biol* **102**, 277-286 (2017).

45. Vogt, T.K., Link, A., Perrin, J., Finke, D. & Luther, S.A. Novel function for interleukin-7 in dendritic cell development. *Blood* **113**, 3961-3968 (2009).

46. Grzesiak, M. *et al*. Serotonin-Related Gene Variants in Patients with Irritable Bowel Syndrome and Depressive or Anxiety Disorders. *Gastroenterol Res Pract* **2017**, 4290430 (2017).

47. Kumar, A. *et al.* The Serotonin Neurotransmitter Modulates Virulence of Enteric Pathogens. *Cell Host Microbe* **28**, 41-53 e48 (2020).

48. Alenina, N. *et al.* Growth retardation and altered autonomic control in mice lacking brain serotonin. *Proc Natl Acad Sci U S A* **106**, 10332-10337 (2009).

49. Moyat, M. *et al.* Microbial regulation of intestinal motility provides resistance against helminth infection. *Mucosal Immunol* **15**, 1283-1295 (2022).

50. Muller, P.A. *et al*. Crosstalk between Muscularis Macrophages and Enteric Neurons Regulates Gastrointestinal Motility. *Cell* **158**, 1210 (2014).

51. Pohl, J.M. *et al.* Irf4-dependent CD103(+)CD11b(+) dendritic cells and the intestinal microbiome regulate monocyte and macrophage activation and intestinal peristalsis in postoperative ileus. *Gut* **66**, 2110-2120 (2017).

52. Furlan, A. *et al*. Visceral motor neuron diversity delineates a cellular basis for nipple- and pilo-erection muscle control. *Nat Neurosci* **19**, 1331-1340 (2016).

53. Jacobson, A., Yang, D., Vella, M. & Chiu, I.M. The intestinal neuro-immune axis: crosstalk between neurons, immune cells, and microbes. *Mucosal Immunol* **14**, 555-565 (2021).

54. Chavan, S.S., Pavlov, V.A. & Tracey, K.J. Mechanisms and Therapeutic Relevance of Neuro-immune Communication. *Immunity* **46**, 927-942 (2017).

55. Quintero-Villegas, A. & Valdes-Ferrer, S.I. Role of 5-HT(7) receptors in the immune system in health and disease. *Mol Med* **26**, 2 (2019).

56. Efremova, M., Vento-Tormo, M., Teichmann, S.A. & Vento-Tormo, R. CellPhoneDB: inferring cell-cell communication from combined expression of multi-subunit ligand-receptor complexes. *Nat Protoc* **15**, 1484-1506 (2020).

57. Drokhlyansky, E. *et al.* The Human and Mouse Enteric Nervous System at Single-Cell Resolution. *Cell* **182**, 1606-1622 e1623 (2020).

58. Fu, R. *et al*. clustifyr: an R package for automated single-cell RNA sequencing cluster classification. *F1000Res* **9**, 223 (2020).

59. Zhao, Y. *et al*. TPM, FPKM, or Normalized Counts? A Comparative Study of Quantification Measures for the Analysis of RNA-seq Data from the NCI Patient-Derived Models Repository. *J Transl Med* **19**, 269 (2021).

60. Kulkarni, S.K., Singh, K. & Bishnoi, M. Elevated zero maze: a paradigm to evaluate antianxiety effects of drugs. *Methods Find Exp Clin Pharmacol* **29**, 343-348 (2007).

61. Woting, A. & Blaut, M. Small Intestinal Permeability and Gut-Transit Time Determined with Low and High Molecular Weight Fluorescein Isothiocyanate-Dextrans in C3H Mice. *Nutrients* **10** (2018).

62. Bolyen, E. *et al*. Reproducible, interactive, scalable and extensible microbiome data science using QIIME 2. *Nat Biotechnol* **37**, 852-857 (2019).

63. Czeloth, N., Bernhardt, G., Hofmann, F., Genth, H. & Forster, R. Sphingosine-1-phosphate mediates migration of mature dendritic cells. *J Immunol* **175**, 2960-2967 (2005).

64. Zhang, H.L. *et al*. Regulatory T-cell depletion in the gut caused by integrin beta7 deficiency exacerbates DSS colitis by evoking aberrant innate immunity. *Mucosal Immunol* **9**, 391-400 (2016).

65. Mach, N. *et al*. Differences in dendritic cells stimulated in vivo by tumors engineered to secrete granulocyte-macrophage colony-stimulating factor or Flt3-ligand. *Cancer Res* **60**, 3239-3246 (2000).

Acknowledgments:
We thank members of the Waldor lab and Drs. Brandon Sit and Susan M. Dymecki for helpful discussions on all aspects of this project, Dr. Gerard Karsenty at Columbia University for *Tph2*$^{-/-}$ mice, Dr. Ulrich H. Von Andrian at Harvard Medical School for the B16-FLT3L cell line, and Dr. Olga Alekseenko and Dr. Barbara Caldarone at the Harvard Mouse Behavior Core for assistance with mouse behavioral testing.

Research in the M.K.W. laboratory is supported by HHMI and NIH grant R01 AI-042347.

Author contributions:

Conceptualization: H.L.Z., R.P.J. and M.K.W.
Methodology: H.L.Z., Y.H., D.R.L., T.Z., and M.S.
Investigation: H.L.Z., Y.H., D.R.L., T.Z., and M.S.
Visualization: H.L.Z., Y.H., D.R.L., T.Z., and M.S.
Funding acquisition: M.K.W.
Supervision: M.K.W.
Writing – original draft: H.L.Z.
Writing – review & editing: H.L.Z. and M.K.W.

Competing interests:
The authors declare no competing interests.

License information:
This article is subject to HHMI's Open Access to Publications policy. HHMI lab heads have previously granted a nonexclusive CC BY 4.0 license to the public and a sublicensable license to HHMI in their research articles. Pursuant to those licenses, the author-accepted manuscript of this article can be made freely available under a CC BY 4.0 license immediately upon publication.

Supplementary Materials:

Datasheet S1, Oligos that were used in this study.
Movie S1, The territorial aggressive behavior assay of WT and whole-body *Tph2* KO mice.

Movie S2, The territorial aggressive behavior assay of *Tph2*$^{fl/fl}$ and *Tph2*$^{fl/fl}$*; Hand2-Cre* mice.

Figure legend.

Figure 1. Detection of enteric serotonergic neurons expressing *Tph2* and creation of a conditional KO mouse lacking *Tph2* in peripheral neurons.

(A) scRNA-seq uniform manifold approximation and projection (UMAP) of Tph2+ enteric neurons from the small intestine of infant mice. Left, subtypes of enteric neurons according to [57]; PSN, putative sensory neurons; PIN, putative inhibitory neuron; PIMN, putative inhibitory motor neurons; PEMN, putative excitatory motor neurons; PSVN, putative secretomotor/vasodilator neurons were defined according to [57]. Right, distribution of Tph2 transcripts among subsets of enteric neurons.

(B) Detection of *Tph2*, *Hand2* and *Tph1* in bulk RNA-seq analysis of the intestinal epithelium, lamina propria immune cells and enteric neurons (n = 9 mice); TPM, Transcripts Per Million.

(C) RT-qPCR analysis of *Tph2* gene expression in the brainstem and the muscularis propria of the small intestine from mice of the indicated genotype (n = 4 mice/group).

Data shown are means ± SD. Statistical analysis was performed by two-tailed unpaired Student's *t*-test in C.

Figure 2. PSN regulate specific aspects of behavior.

(A) Open field test measures of total distance traveled, and time spent in the center area of the open field in mice of the indicated genotypes (WT, n = 21; *Tph2*$^{-/-}$, n = 20; *Tph2*$^{fl/fl}$, n = 16; and *Tph2*$^{fl/fl}$; *Hand2-Cre*, n = 16).

(B) Resident-intruder assay measures of the latency to the first attack, number of attack bites and cumulative attack duration by WT (n = 13) and *Tph2*$^{-/-}$ (n = 11) as well as *Tph2*$^{fl/fl}$ (n = 12) and *Tph2*$^{fl/fl}$; *Hand2-Cre* (n = 12) mice.

(C) Elevated plus maze assay measures of the total distance traveled, and time spent in the open arms by WT (n = 18) and *Tph2*$^{-/-}$ (n = 21) as well as *Tph2*$^{fl/fl}$ (n = 15) and *Tph2*$^{fl/fl}$; *Hand2-Cre* (n = 17) mice.

(D) Elevated zero maze (EZM) measures of time spent in the open arms for WT (n = 13), *Tph2*$^{-/-}$ (n = 11), *Tph2*$^{fl/fl}$ (n = 12), and *Tph2*$^{fl/fl}$; *Hand2-Cre* (n = 12).

Data shown are means ± SD. Statistical analysis was performed by two-tailed Mann-Whitney test in A-D.

Figure 3. PSN control gut motility and the abundance of intestinal dendritic and IgA B cells.

(A) Total GI transit time was measured using carmine red assay in WT (n = 9) and *Tph2*$^{-/-}$ (n = 8) as well as *Tph2*$^{fl/fl}$ (n = 10) and *Tph2*$^{fl/fl}$; *Hand2-Cre* (n = 12) mice.

(B) Differential gene expression of CD45+ cells isolated from the lamina propria of the small intestine from co-housed WT and *Tph2*$^{-/-}$ mice. Red points indicate increased expression and blue points indicate decreased expression in *Tph2*$^{-/-}$ mice compared to WT mice.

(C, D) Flow cytometry analyses of frequency of DC (Live, CD45+, MHC-II+, CD64-, CD11c+) in lamina propria CD45+ cells from the small intestine of mice with the indicated genotypes (n = 9) (C), and the frequency of total B cells, IgD+ fraction of total B cells, and IgA+ cells in the lamina propria CD45+ cells from the small intestine of mice with indicated genotypes (n = 9) (D).

(E) Fecal IgA levels in mice with the indicated genotypes (n = 21 mice per group).

(F) Representative immunostaining of small intestine sections from mice of indicated genotypes. Epithelial cells are detected with EpCAM (magenta), IgA cells with anti-IgA antibody (green), and nuclei with DAPI (blue). Scale bar, 100 μm.

Data shown are means ± SD. Statistical analysis was performed by two-tailed Mann-Whitney test in A, and C-E.

Figure 4. Serotonin remodels DC function to promote IgA+ B cell differentiation.

(A) *Htr7* is the dominant serotonin receptor in LPDC. FPKM (Fragments Per Kilobase of transcript per Million fragments mapped) values of all serotonin receptors in LPDC.

(B) UMAP plot of single-cell transcriptome data [32] of small intestinal lamina propria immune cells showing that expression of the *Htr7* gene is restricted to LPDC cells.

(C) Differential gene expression in LPDCs treated with serotonin ±*Htr7* antagonist. Red and blue points indicate genes whose expression was significantly increased or decreased respectively, in a *Htr7*-dependent fashion.

(D) Gene Ontology pathways analysis of data from C.

(E) Tissue culture assay of IgA production from IgD+ B cells that were cocultured with LPDC, serotonin, and a *Htr7* antagonist (SB269970) as indicated. The levels of IgA in the supernatants were measured by ELISA after 6 days of culture (n = 12). Data are representative of three independent experiments.

Data shown are means ± SD. Statistical analysis was performed by two-tailed Mann-Whitney test in E.

Figure 5. PSN remodel LPDC function *in vivo*.

(A) UMAP plot of single-cell transcriptome data of small intestinal LPDCs from *Tph2*$^{fl/fl}$ and *Tph2*$^{fl/fl}$*; Hand2-Cre* mice.

(B) Pie charts showing the proportion of cluster 0 and 4 cells are decreased in *Tph2*$^{fl/fl}$*; Hand2-Cre* vs *Tph2*$^{fl/fl}$ mice.

(C) Violin plots depicting the range of expression levels of *Htr7* and *Ccr7* in distinct LPDC clusters.

(D) UMAP plot derived from single-cell transcriptome data showing expression of *Htr7* and *Ccr7* in LPDCs from *Tph2*$^{fl/fl}$ and *Tph2*$^{fl/fl}$*; Hand2-Cre* mice. The color scale represents relative expression level.

(E) Comparison of the expression of the indicated genes in cluster 0 of LPDC between *Tph2*$^{fl/fl}$ and *Tph2*$^{fl/fl}$*; Hand2-Cre* mice. Dot color reflects the level of gene expression and dot size represents the percentage of cells expressing the indicated gene. The genes labeled in red are decreased in cluster 0 of LPDC in *Tph2*$^{fl/fl}$*; Hand2-Cre* mice and are consistent with the serotonin-induced genes observed *in vitro*.

(F) Schematic of the system used to analyze BMDC homing to the gut in *Tph2*$^{fl/fl}$ and *Tph2*$^{fl/fl}$*; Hand2-Cre* mice. Equal numbers of CFSE-labeled mature BMDCs were transplanted into *Tph2*$^{fl/fl}$ and *Tph2*$^{fl/fl}$*; Hand2-Cre* mice, and the CFSE+ cells in different tissues was analyzed 18 h post-transplantation.

(G) Frequency of CFSE+ cells among CD45+ cells in the lamina propria of *Tph2*$^{fl/fl}$ and *Tph2*$^{fl/fl}$*; Hand2-Cre* mice (n = 9).

Data shown are means ± SD. Statistical analysis was performed by two-tailed Mann-Whitney test in G.

Figure 6. PSN boost host defense.

(A-B) Salmonella typhimurium (Stm) CFU burdens in livers and spleens of mice with the indicated genotypes (WT, n = 15; *Tph2*$^{-/-}$, n = 17; *Tph2*$^{fl/fl}$, n = 12; and *Tph2*$^{fl/fl}$; *Hand2-Cre*, n = 12) 5 days post oral inoculation.

(C-D) Kaplan Meier plot of survival of mice of indicated genotypes following oral Salmonella inoculation (n = 16).

(E) Kaplan Meier plot of survival of WT and *Tph2*$^{-/-}$ mice after intravenous Salmonella infection (n = 14). Data shown are means ± SD. Statistical analysis was performed by two-tailed Mann-Whitney test in A, B; and by Log-rank test in C-E.

Figure 7. Bidirectional communication between enteric neurons and LPDCs.

(A) UMAP plot of single-cell transcriptome data of enteric neurons and lamina propria dendritic cells generated in this study that was used for analyzing cell-cell communication with CellChat.

(B) Circle network diagram of significant cell-cell interaction pathways. Arrows and line color indicate direction (ligand: receptor) and line thickness indicates the strength of the predicted interaction. The round loops represent the interactions within the same cell type.

(C) Heatmap showing the two global communication patterns calculated by the key signals for subpopulations between enteric neurons and LPDC cells.

(D-F) Enteric neuron to LPDC communication pathways. (D) Chord diagram showing all the significant interactions from enteric neuron to LPDC. (E) Dot plot showing the key ligand-receptor interactions in inferred communication pathways between subsets of enteric neurons and LPDC. Empty spaces indicate that the communication probability is zero. p-values were computed with a one-sided permutation test. The color scale represents communication probability as calculated in CellChat. (F) Violin plots illustrating the gene expression levels of the Ptn signaling pathway, with ligand expression in enteric neuron clusters and receptor expression in LPDC clusters.

(G-I) LPDC to enteric neuron communication pathway. (G) Chord diagram showing all the significant interactions from LPDC to enteric neuron. (H) Dot plot showing the key ligand-receptor interactions in inferred communication pathways between subsets of LPDC and enteric neurons. Empty spaces indicate that the communication probability is zero. p-values were computed with a one-sided permutation test. The color scale represents communication probability as calculated in CellChat. (I) Violin plots illustrating the gene expression levels of the

Nampt-Insr signaling pathway, with ligand expression in LPDC clusters and receptor expression in enteric neuron clusters.

(J) Chord diagram displaying the communication network between enteric neuron cluster 4 and LPDC cluster 0, highlighting the targeting of *Il7* from the former cell population to the *Il7r* located on the latter cell population.

(K) Violin plots illustrating the gene expression levels in distinct cell subtypes. Violin plot illustrating the gene expression levels of the IL7 signaling pathway, with ligand expression in enteric neuron cluster 4 and receptor (a heterodimer of *Il7r* and *Il2rg*) expression in LPDC cluster 0.

(L) UMAP plot derived from single-cell transcriptome data showing expression of *Il7* in enteric neuron cluster 4 and Il7 receptor in LPDC cluster 0.

Figure S1. Detection of intestinal *Tph2* expressing neurons.

(A-B) Comparison of enteric neuron subtypes detected in this study with those in [57]. The color scale in the heatmap in (A) represents Spearman's rank correlation coefficients between the cell clusters found in this study and the reference cell types in [57]. The UMAP in (B) shows the correspondence of the clusters found in our study with those in [57].

(C) UMAP shows the majority of *Tph2*+ cells are *Ret*+ enteric neurons.

(D) Immunofluorescent staining of the small intestine myenteric plexus with AF647 conjugated anti-Tuj1 antibody; scale bar, 100 μm.

(E) RT-qPCR analyses of the expression of neuronal marker genes in the small intestine muscularis propria from $Tph2^{fl/fl}$ and $Tph2^{fl/fl}$*; Hand2-Cre* mice (n = 4 mice/group).

Data shown are means ± SD. Statistical analysis was performed by two-tailed unpaired Student's *t*-test in E.

Figure S2. PSN regulate gut motility but do not have a major impact on the intestinal epithelium or the composition of the microbiota.

(A) FITC-dextran assay of small intestinal motility in *Tph2*$^{fl/fl}$ (n = 7) and *Tph2*$^{fl/fl}$; *Hand2-Cre* (n = 6) mice. Data shown are means ± SD. Statistical analysis was performed by two-tailed Mann-Whitney test.

(B) Periodic Acid-Schiff stain (PAS) staining of the small intestine and colon of *Tph2*$^{fl/fl}$ and *Tph2*$^{fl/fl}$; *Hand2-Cre* mice. Scale bars, 100 μm.

(C) *Htr4* is the dominant serotonin receptor in small intestinal epithelial cells. FPKM (Fragments Per Kilobase of transcript per Million fragments mapped) values of all serotonin receptors in small intestinal epithelial cells.

(D) UMAP plot derived from single-cell transcriptome data in Tsang et al [30] showing expression of *Htr4* in epithelial cells (Vil1+) in the small intestine.

(E-F) Comparison of gene expression in the small intestinal (E) and colonic (F) epithelium of co-housed WT and *Tph2*$^{-/-}$ mice.

(G-H) Bar plot of microbiota taxa at the genus and species level in mice with indicated genotypes (n = 6).

(I-J) Comparison of gene expression in the small intestinal (I) and colonic epithelium (J) of separately housed WT and *Tph2*$^{-/-}$ mice. Red points indicate increased expression and blue points indicate decreased expression in *Tph2*$^{-/-}$ mice compared to WT mice.

Figure S3. PSN regulate intestinal immune homeostasis.

(A) Gene Ontology pathways analysis of data from Figure 3B.

(B) Differential gene expression of CD45+ cells in the lamina propria of the colon from co-housed WT and *Tph2*$^{-/-}$ mice.

(C) Gating strategy for detection and sorting of different immune cell types. B cells were gated as live CD45+ CD19+; IgD cells were gated as live CD45+ CD19+ IgD+; IgA cells were gated as live CD45+ IgA+; DCs were gated as live CD45+ MHCII+ CD64- CD11c+.

(D) Flow cytometry analysis of the frequency of CD3+ in CD45+ cells and CD8+ in CD3+ T cells in the lamina propria of the small intestine from co-housed *Tph2*$^{fl/fl}$ and *Tph2*$^{fl/fl}$; *Hand2-Cre* mice (n = 5).

(E) Quantification of IgA+ cells per field from nine fields per group (n = 3 mice per group).

(F) Flow cytometry analysis of the frequency of IgA+ cells in CD45+ cells from the MLN and PP from co-housed *Tph2*$^{fl/fl}$ and *Tph2*$^{fl/fl}$; *Hand2-Cre* mice (n = 5).

Data shown are means ± SD. Statistical analysis was performed by two-tailed Mann-Whitney test in D-F.

Figure S4. Serotonin regulates LPDC gene expression through 5-HT$_7$ receptor.

(A-B) Expression of select genes in LPDCs after treatment with serotonin ±*Htr7* antagonist (n = 4). Data shown are means ± SD. Statistical analysis was performed by two-tailed unpaired Student's *t*-test in A and B.

Figure S5. PSN remodel LPDC function *in vivo*.

(A) UMAP plot of single-cell transcriptome data of cells by DC selected from the small intestine lamina propria from *Tph2*$^{fl/fl}$ mice. Clusters 2, 6-8, 11, 12, 14, 15, 17, 18, which did not express *H2-Ab1* (MHC-II) were computationally removed to create the UMAP in B.

(B) UMAP plots comparing the abundance of MHC-II positive clusters of DC in *Tph2*$^{fl/fl}$*; Hand2-Cre* compared with *Tph2*$^{fl/fl}$ mice. The conditional KO animals had decreased proportions of DC (cluster 1, 3, 4, 5, and 6 defined by Cd11c+).

(C) Pie charts show decreased proportions of LPDC (Cluster 1, 3, 4, 5, and 6) in *Tph2*$^{fl/fl}$*; Hand2-Cre* compared with *Tph2*$^{fl/fl}$ mice (64.6% vs 45.5%).

(D) Frequency of CFSE+ cells among CD45+ cells in the MLN and PP of *Tph2*$^{fl/fl}$ and *Tph2*$^{fl/fl}$*; Hand2-Cre* mice (n = 5).

Data shown are means ± SD. Statistical analysis was performed by two-tailed unpaired Student's t-test in D.

(E) Schematic of ESN-DC interaction. Serotonin secreted by enteric serotonergic neurons activate LPDCs through 5-HT7 receptor via a synapse-like mechanism or an indirect pathway that leads to increased expression of genes crucial for DC-mediated differentiation of IgA+ B cells from precursor IgD+ cells.

Figure S6. Bidirectional communication between enteric neurons and LPDCs.

(A) UMAP plot derived from single-cell transcriptome data showing expression of indicated genes in enteric neurons (left population) and LPDCs (right population).

(B) UMAP plot derived from single-cell transcriptome data showing expression of *Ptn* in enteric neurons and its receptor *Ncl* in LPDCs.

(C) UMAP plot derived from single-cell transcriptome data showing expression of *Nampt* in LPDCs and its receptor *Insr* in enteric neurons.

(D) 5-HT_{3a} is the dominant serotonin receptor in enteric neurons. FPKM (Fragments Per Kilobase of transcript per Million fragments mapped) values of all serotonin receptors in enteric neurons.

(E) UMAP plot derived from single-cell transcriptome data showing expression of *Htr3a* in enteric sensory neurons in cluster 0 in Figure S1B.

RESOURCE AVAILABILITY

Lead contact

Please direct requests for resources and reagents to Lead Contact, Matthew K. Waldor (mwaldor@research.bwh.harvard.edu).

Materials availability

This study did not generate new unique reagents.

Data availability

All scRNA-seq, bulk RNA-seq datasets and 16S sequencing data generated here have been deposited into the NCBI Gene Expression Omnibus database under accession number GSE227340.

EXPERIMENTAL MODEL AND SUBJECT DETAILS

Mice. C57BL/6, Tg(*Uchl1*-HISTH2BE/mCherry/EGFP*)Fsout/J, and *Tph2*$^{flox/flox}$ mice were purchased from the Jackson Laboratory (Bar Harbor, ME, USA); Swiss Webster (CFW) mice were purchased from the Charles River Laboratories (Wilmington, MA, USA); *Tph2*$^{-/-}$ mice were a generous gift from Dr. Gerard Karsenty (Columbia University, NY, USA); *Hand2-Cre* transgenic mice were a generous gift from Ruaidhrí Jackson (Harvard Medical School, MA, USA). *Tph2*$^{flox/flox}$ mice were backcrossed to C57BL/6J background for at least six generations. All mice were maintained on a 12-hour light/dark cycle and a standard chow diet at the Harvard Institute of Medicine specific pathogen-free (SPF) animal facility. Animal experiments were performed according to guidelines from the Center for Animal Resources and Comparative Medicine at Harvard Medical School. All protocols and experimental plans were approved by the

Brigham and Women's Hospital Institutional Animal Care and Use Committee (Protocol #2016N000416).

Isolation and purification of nuclei from enteric neurons.

The isolation of enteric neurons from Tg(*Uchl1*-HISTH2BE/mCherry/EGFP*)Fsout/J mice was performed as previously described[57]. Briefly, fresh-frozen intestinal tissues were disaggregated in 1 mL of CST buffer (0.49% (w/v) CHAPS (220201, EMD Millipore), 146 mM NaCl (S6546, Sigma), 1mM $CaCl_2$ (97062-820, VWR), 21 mM $MgCl_2$ (M1028, Sigma), 10 mM Tris pH 8.0 (AM9855G, Thermo Fisher) with mild chopping using scissors for 10 minutes on ice. Large debris were removed with a 40 μm strainer (Falcon). The isolated nuclei were stained with 4',6-diamidino-2-phenylindole (DAPI, D1306, Thermo Fisher Scientific) and sorted as DAPI+, mCherry+ nuclei using a SH800 Cell Sorter (Sony Biotech). The purified nuclei were used for single-nucleus RNA-seq or bulk RNA-seq analysis.

Intestinal epithelium and immune cell isolation and purification.

Colonic and small intestinal tissues were dissected, and Peyer's patches discarded. The epithelium was isolated by 250 rpm stirring at 37 °C in RPMI medium (61870036, Gibco) containing 5 mM EDTA (AM9260G, Invitrogen), 1 mM dithiothreitol (10197777001, Sigma) and 2% (vol/vol) FBS (10082147, Gibco) for 15 min. The isolated epithelium was used for bulk RNA-seq analysis.

To isolate lamina propria lymphocytes, the epithelium-depleted intestinal tissues were washed in RPMI medium with 5% (vol/vol) FBS, further minced into small pieces, and then digested by 250 rpm stirring at 37 °C in RPMI medium containing collagenase D (0.5 mg/ml, 11088866001, Sigma), Dispase II (0.5 mg/ml, 17105041, Gibco), DNase I (50 ug/ml, 10104159001, Roche) and 5% (vol/vol) FBS for 40 min. The digested tissues were filtered, and lamina propria cells were collected by centrifugation. The pellets were resuspended, and the

lamina propria lymphocytes were isolated by Percoll (40%/80%, GE17-0891-01, GE Healthcare) gradient centrifugation. Mesenteric lymph nodes and Peyer's patches were mechanically disrupted. The purified immune cells were used for FACS analysis and sorting. The sorted $CD45^+$ cells and dendritic cells were used for bulk RNA-seq analysis.

FACS analysis and cell sorting.

Single-cell suspensions were blocked with an antibody against CD16/32 (2.4G2, Becton Dickinson) and then stained with LIVE/DEAD™ fixable aqua cell stain kit (L34957, Invitrogen) and antibodies against CD45 (30-F11), MHC-II (M5/114.15.2), CD64 (X54-5/7.1), CD11c (HL3), B220 (RA3-6B2), IgD (11-26c), and IgA (C10-3) all from Becton Dickson. Stained cells were analyzed with a FACSymphony analyzer (Becton Dickson) or sorted on a SH800 Cell Sorter; analyses were performed with FlowJo software (v10.8).

Single nucleus RNA-Seq.

The 10× Genomics protocol was performed on single sorted enteric nucleus as described [57]. Libraries were generated using Chromium Next GEM Single Cell 3 Reagent Kits v3.1 (10×) according to the manufacturer's protocol; library quality was assessed by the Tapestation High Sensitivity D5000 ScreenTape (Agilent) and sequenced using a NextSeq 500 sequencer (Illumina). Data analysis was performed using the 10× Genomics Cloud Analysis Cell Ranger pipeline and Seurat v4.3.0 with the SCT normalization method. Low quality cells were removed by the parameters nfeature_RNA > 500, nCount_RNA > 2000 & nCount_RNA < 50000, and percent.mt < 5. To generate UMAPs, we integrated our data with published small intestine data in Drokhlyansky et al.[57] and performed a principal component analysis (PCA) using RunPCA function (npcs=50), and then cell clusters were identified using FindNeighbors (dims=1:15) and FindClusters (resolution=0.4) functions. RunUMAP function (dims=1:15, n.neighbors=15, min.dist=0.3, spread=1) was used to create UMAP plots. The cell-type assignment was

performed using clustifyr R package (v1.8.0, clustifyr[58]) based on the cell-types presented in Drokhlyansky et al[57].

Single cell RNA-Seq of LPDC.

Lamina propria lymphocytes were purified on percoll gradients from *Tph2*$^{fl/fl}$ and *Tph2*$^{fl/fl}$*; Hand2Cre* mice and then DC were isolated using the EasySep™ Mouse CD11c Positive Selection Kit II (18781, StemCell). Library generation, sequencing and data analysis was performed as described above. MHC negative cell clusters were computationally removed prior to analyses of MHC+ cell clusters. LPDC cell clusters specific analyses were carried out after computational removal of Cd11c negative cell clusters.

Bulk RNA-seq and data analysis.

Purified epithelial and immune cells were lysed in Trizol (15596018, Invitrogen), and RNA was extracted with the RNeasy mini Kit (74106, Qiagen) according to the manufacturer's instructions. RNA-seq libraries were prepared using the KAPA mRNA HyperPrep kit (50-196-5308, Roche) or NEBNext Multiplex Oligos for Illumina kit (E7335L, NEB). Libraries were analyzed using a High Sensitivity D1000 ScreenTape (Agilent) and sequenced on a NextSeq 550 or 1000/2000 (Illumina). For data analysis, reads were trimmed using Trim Galore with automatic adapter sequence detection. Then, trimmed reads were mapped to the mouse reference genome (mm10) and annotated using STAR v2.7.3a with default parameter. The number of mapped reads to each gene were counted by featureCounts of the Subread package using mouse GENCODE annotation M25 (GRCm38.p6). Transcripts Per Kilobase Million (TPM) was calculated by dividing the number of read counts by the length of the gene in kilobases to yield reads per kilobase. Fragments Per Kilobase of transcript per Million fragments mapped (FPKM) was also calculated as described[59]. Differentially expressed genes were identified using the R-package DESeq2 (v1.36.0) with adjusted p-value < 0.05.

Mouse behavior assays.

The following assays were carried at the Harvard Medical School Mouse Behavior Core according to standard methods by an observer blinded to the genotype of the animal:

Open Field: a large arena (50 × 50 cm) under low illumination (30 lux) was used as an open field to measure locomotor activity. Each mouse was placed into the arena and its activity was measured during 10 min. The total distance traveled, and time spent in the center were calculated.

Resident-intruder assay: This assay was performed largely as described[29]. Transgenic male mice, ‘‘residents’’ were group-housed with male siblings until sexual maturity. Resident males were assayed for aggression toward a wild-type Swiss Webster (CFW) (Charles River) intruder mouse. Each intruder mouse was used only once to avoid submissive/dominance effects after the initial interaction. Behavioral interactions during each confrontation were recorded and subsequently scored by an observer blinded to the mouse genotype. Latency to the first attack, total amount of attacks and cumulative duration of attacks were analyzed.

Elevated plus maze (EPM) and zero maze (EZM): The EPM and EZM test is based on the aversion of rodents to open, bright illuminated spaces[60]. The EPM consisted of two open arms (30 × 5 cm) and two closed arms (30 × 5 cm) that were enclosed by a sidewall on all edges (height 15cm). The EZM consisted of a gray plastic annular runway (width 6 cm, outer diameter 46 cm, 50 cm above ground level). Two opposing sectors were protected by inner and outer walls of gray polyvinyl (height 15 cm). Mice were placed in one of the protected sectors of the maze facing the closed arm. Distance travelled and time spent in open arms were quantified

during 10 min tests. Arm entry was only scored when an animal (the mouse mass center) was at least 3 cm in an arm.

Gut motility assays.

Total gastrointestinal transit time: Carmine red, which cannot be absorbed from the lumen of the gut, was used to study total GI transit time. A solution of carmine red (200 μl; 6%; C1022, Sigma) suspended in 0.5% methylcellulose (M0512, Sigma) was administered by gavage through a 21-gauge round-tip feeding needle. The time at which gavage was carried out was recorded as T0. After gavage, fecal pellets were monitored at 10 min intervals for the presence of carmine red. Total GI transit time was calculated as the interval between T0 and the time of first observance of carmine red in stool.

Small intestine transit time: A solution containing fluorescein isothiocyanate-dextran (FITC-Dextran, 100 μl; 10 mg/ml in 2% methylcellulose; FD70, Sigma) was administered to mice by gavage through a 21-gauge round-tip feeding needle. Animals were sacrificed 15 min after gavage; the small intestine, cecum, and colon were collected in PBS. The small intestine was divided into 10 segments of equal length, and the colon was divided in half. Each piece of tissue was transferred into a 2 ml tube containing 1 ml of PBS, homogenized, and centrifuged (2000 × g), yielding a clear supernatant. FITC fluorescence was measured in the supernatant (Epoch2, Biotek). Small intestinal transit was estimated by the position of the geometric center of the FITC-dextran in the small bowel as described[61] . For each segment of the small intestine (1-10), the geometric center (a) was calculated as follows: a = (fluorescence in each segment × number of the segment)/(total fluorescence recovered in the small intestine). The total geometric center is Σ (a of each segment) and was normalized to WT littermates.

Histology and tissue immunofluorescence. Paraformaldehyde (PFA)-fixed, paraffin-embedded sections of small intestine and colon samples of 4 μm thickness were mounted on glass slides and stained with Periodic acid-Schiff stain. For immunofluorescence analysis, samples from the small intestine were collected and flushed with PBS and fixed in 4% PFA followed by washing with PBS. Tissue samples were then soaked in 30% sucrose and embedded in Optimal Cutting Temperature Compound (23-730-571, Fisher Scientific) and stored at -80°C before sectioning on a CM1860 UV cryostat (Leica). 8 μm-thick slides were stained with FITC-anti IgA (C10-3, Becton Dickson) and Percp/cy5.5 anti-EpCAM (G8.8, Biolegend) antibodies at 4°C overnight at a 1:200 dilution in PBS. Nuclei were stained with DAPI at RT for 5 min in the dark. For staining of myenteric plexuses, a small segment of the proximal small intestine was removed and placed in ice-cold PBS and then transferred to a Sylgard (Dow-Corning)-coated Petri dish. The intestine was opened along the mesenteric border and pinned flat, and then the mucosa, submucosa was removed with forceps to expose the muscularis propria layer. The resulting muscularis propria preparation was stained overnight with Alexa Fluor 647 anti-Tubulin β3 antibody (TUJ1, Biolegend) and rinsed in PBS before imaging with an Eclipse Ti confocal microscope with a 20 × objective (Nikon).

ELISA for fecal IgA.

Fresh mouse feces were homogenized in 10 × volume (v/w) of PBS containing the protease inhibitor cocktail Complete EDTA-free (11836153001, Roche), using a bead-beater (Biospec, Bartlesville, OK, USA) for 20 sec, and the centrifuged at 3,000 rpm for 15 min at 4°C. Supernatants were further spun down at 10,000 rpm for 5 min at 4°C, and the IgA level in the final supernatant was determined using the Mouse IgA ELISA kit (88-50450-86, Thermo Fisher Scientific) according to the manufacturer's protocol.

RT-qPCR quantification of gene expression.

The brainstem and small intestine muscularis propria were isolated and lysed in Trizol (15596018, Invitrogen). RNA was purified with the RNeasy mini Kit (74106, Qiagen) according to the manufacturer's instructions. RNA samples were treated for residual DNA contamination using Ambion Turbo DNA-free DNase (AM1907, Invitrogen). Purified RNA was reverse transcribed for quantitative RT-PCR (RT-qPCR) by adding 10 μg of total RNA to a mixture containing oligo dT (N8080128, Thermo Fisher scientific), 25 mM dNTPs (R0191, Thermo Fisher Scientific), 0.01 M dithiothreitol, reaction buffer and 200 units of SuperScript III reverse transcriptase (18080085, Invitrogen). cDNA was diluted 1:50 in dH2O and mixed with an equal volume of target-specific primers and Roche SYBR master mix (04707516001, Roche) or TaqMan™ Gene Expression Master Mix (4369016, Applied Biosystems). Primer pairs were designed to minimize secondary structures and a melting temperature of 60°C using the primer design software Primer 3. Primer sequences are listed in Dataset S1. For data normalization, quadruplicate Ct values for each sample were averaged and normalized to Ct values of the control gene *Gapdh*. The relative gene expression level was determined by normalizing to expression in the WT.

16S rRNA profiling of the gut microbiota.

Fecal DNA was extracted from mouse fecal pellets with the QIAGEN QIAamp Fast DNA Stool Mini Kit (51604, Qiagen) according to the manufacturer's instructions. Purified DNA samples were amplified with barcoded primer pairs: 341F and 805R. The amount of PCR products were quantified with the Qubit kit (Q32854, Invitrogen) and then the same amount of DNA from each sample was pooled for sequencing on MiSeq (Illumina). Raw sequencing data were analyzed by QIIME2[62]. In brief, the data were imported into QIIME2 and demultiplexed and the DADA2 pipeline was used for sequencing quality control, and a feature table was constructed. The feature

table was used for alpha and beta diversity analysis as well as for taxonomic analysis and differential abundance testing.

BMDC gut homing assay.

Bone marrow-derived dendritic cells (BMDCs) were generated from a flushed bone marrow suspension as previously described[63]. In brief, 5×10^6 bone marrow cells from the femurs of C57BL/6J mice were cultured in 10 ml medium containing RPMI 1640 (11875093, Gibco) with 10% FBS (10082147, Gibco), β-Mercaptoethanol (21985023, Gibco), GlutaMAX (35050061, Gibco) and penicillin-streptomycin (10378016, Gibco) supplemented with 100 ng/ml granulocyte-macrophage colony-stimulating factor (GM-CSF; 315-03, PeproTech). Another 10 ml of GM-CSF supplemented medium was added every 3 days. To generate mature BMDCs, 1 µg/ml lipopolysaccharide (LPS; LPS25, Sigma) was added to the cell suspensions on day 8 for 24 h. At day 9, mature BMDCs were harvested, and labeled with CellTrace CFSE (C34554, Thermo Fisher scientific) and then injected intravenously into *Tph2*$^{fl/fl}$ and *Tph2*$^{fl/fl}$*; Hand2-Cre* mice. Recipient mice were sacrificed 18 h after injection, and lymphocytes from tissues were harvested. The number of FITC$^+$ cells in the spleen was used to normalize the amount of input and MLN, PP and lamina propria FITC$^+$ cells were normalized to splenic FITC to compare DC gut homing to different organs in different animals as described[64].

LPDC and IgD$^+$ B cell isolation and co-culture.

C57BL/6J mice were subcutaneously injected with B16 cells secreting Flt3-L as described[65]. After 12 to 14 days, mice were sacrificed and the small intestine lamina propria was digested as described above. Single cell suspensions were incubated with mAbs to CD11c and IgA. Sorted LPDC (> 95% CD11c$^+$ IgA$^-$) were resuspended at 2×10^6/ml and used immediately in co-culture assays. Naïve B cells were purified from the spleen by sorting IgD$^+$ IgA$^-$ cells (> 95% IgD$^+$ IgA$^-$ cells).

For co-cultures of sorted IgD^+ and LPDC cells, IgD^+ B cells were activated with 10 μg/ml anti-mouse IgM F(ab')2 (Poly21571, Biolegend), either alone or plus LPDC (1:1 ratio), treated with or without 100 uM serotonin (14927, Sigma) and/or 1uM *Htr7* antagonist SB 269970 hydrochloride (1612, Tocris) for 7 days. Then the supernatant was collected for IgA measurement as above.

***In vivo Stm* infection.**

Salmonella typhimurium (SL1344, *Stm*) were grown for ~16 h at 37 °C with shaking and then subcultured (1:33) in lysogeny broth (LB) without antibiotics for 3 h until the cultures reached an optical density at 600 nm of 0.8. To prepare the inoculum, cultures were first pelleted at 5,000 × g for 5 min. The pellets were resuspended in PBS. For oral infection, mice were fasting for 4 h before infected orogastrically with 5×10^8 *Stm* suspended in 100 μl PBS. For intravenous infection, mice were infected with 1×10^2 *Stm* suspended in 100 μl PBS via the lateral tail vein. Survival was monitored by daily observation and Kaplan Meier survival graphs were generated by Prism software (GraphPad, version 9.4.1). *Stm* colony-forming units (CFU) in the spleen and liver were measured 5 days after infection by plating serial-dilutions of homogenized tissue samples on LB plates containing 100 μg/ml streptomycin.

Cell-cell interaction analysis.

We used the single-cell RNA-seq data generated from this study to analyze enteric neuron and LPDC interactions using the CellChat package [42]. Data analysis was performed with Seurat v4.3.0 as above except when the data was combined the resolution was set to 0.1 for FindClusters. CellChat identified differentially expressed ligands and receptors from each cell group and associated each interaction with a communication probability. Significant interactions

were identified using default settings in CellChat. The results were visualized using bubble and chordal plots through the netVisual_bubble and chordDiagram functions in CellChat. The CommunicationPatterns function in the CellChat package was used to identify and visualize receptor repertoires.

Statistical methods.

Statistical analyses were carried out using the two-tailed Student's *t*-test, two-tailed Mann-Whitney test or Kaplan-Meier Log-rank test on GraphPad Prism5 (version 9.4.1).

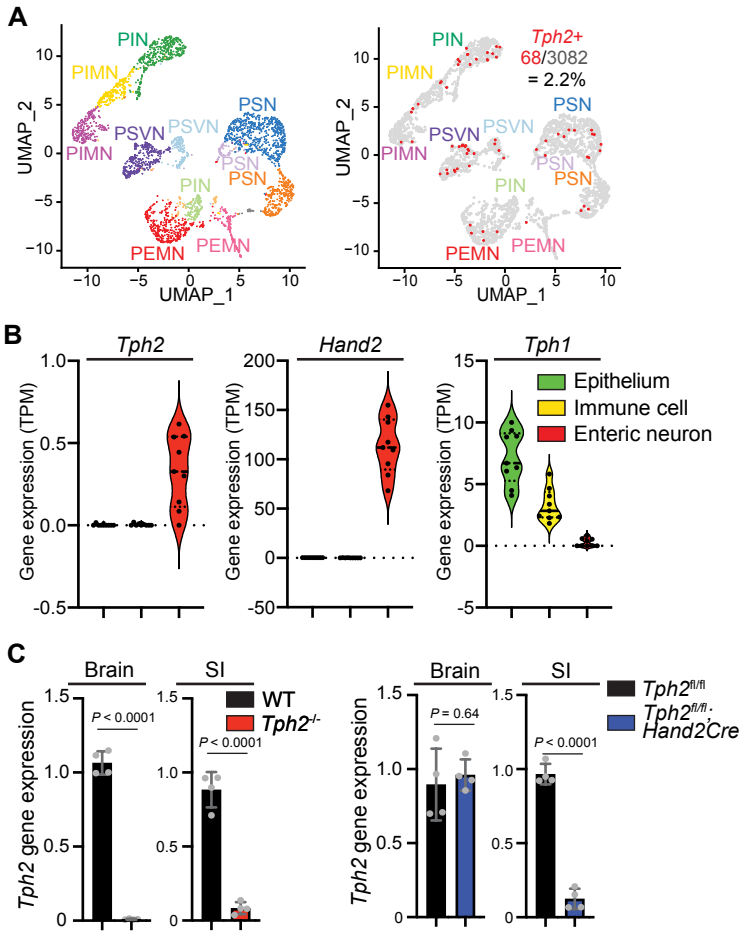

Figure 1. Detection of enteric serotonergic neurons expressing *Tph2* and creation of a conditioal KO mouse lacking *Tph2* in peripheral neurons.

(A) scRNA-seq uniform manifold approximation and projection (UMAP) of *Tph2*⁺ enteric neurons from the small intestine of infant mice. Left, subtypes of enteric neurons according to Drokhlyansky et al.; PuSN, putative sensory neurons; PIN, putative inhibitory neuron; PIMN, putative inhibitory motor neurons; PEMN, putative excitatory motor neurons; PSVN, putative secretomotor/vasodilator neurons were defined according to Drokhlyansky et al. Right, distribution of *Tph2* transcripts among subsets of enteric neurons.
(B) Detection of *Tph2*, *Hand2* and *Tph1* in bulk RNA-seq analysis of the intestinal epithelium, lamina propria immune cells and enteric neurons (n = 9 mice); TPM, Transcripts Per Kilobase Million.
(C) RT-qPCR analysis of *Tph2* gene expression in the brainstem and the muscularis propria of the small intestine from mice of the indicated genotype (n = 4 mice/group).
Data shown are means ± SD. Statistical analysis was performed by two-tailed unpaired Student's *t*-test in C.

Fig. 1

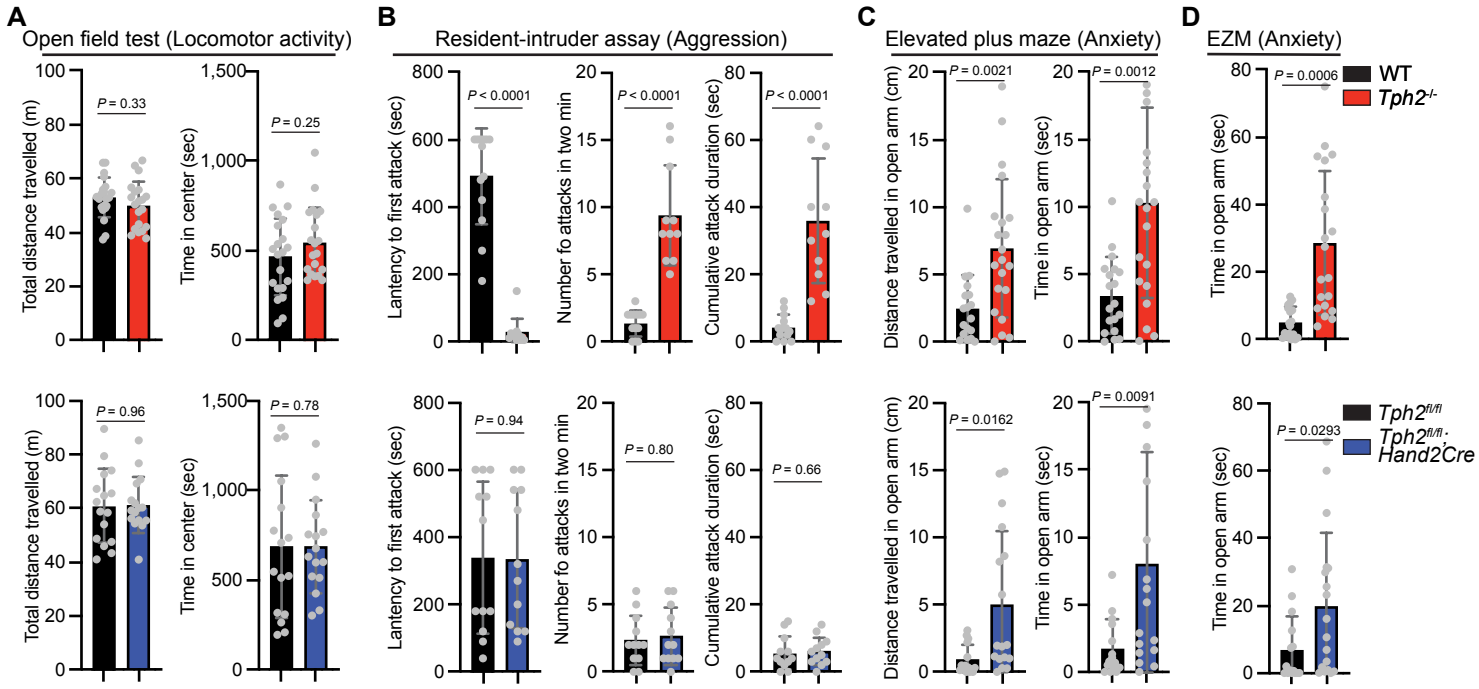

Figure 2. PSN regulate specific aspects of behavior.

(A) Open field test measures of total distance traveled, and time spent in the center area of the open field in mice of the indicated genotypes (WT, n = 21; *Tph2*$^{-/-}$, n = 20; *Tph2*$^{fl/fl}$, n = 16; and *Tph2*$^{fl/fl}$*; Hand2-Cre*, n = 16).

(B) Resident-intruder assay measures of the latency to the first attack, number of attack bites and cumulative attack duration by WT (n = 13) and *Tph2*$^{-/-}$ (n = 11) as well as *Tph2*$^{fl/fl}$ (n = 12) and *Tph2*$^{fl/fl}$; *Hand2-Cre* (n = 12) mice.

(C) Elevated plus maze assay measures of the total distance traveled, and time spent in the open arms by WT (n = 18) and *Tph2*$^{-/-}$ (n = 21) as well as *Tph2*$^{fl/fl}$ (n = 15) and *Tph2*$^{fl/fl}$*; Hand2-Cre* (n = 17) mice.

(D) Elevated zero maze (EZM) measures of time spent in the open arms for WT (n = 13), *Tph2*$^{-/-}$ (n = 11), *Tph2*$^{fl/fl}$ (n = 12), and *Tph2*$^{fl/fl}$*; Hand2-Cre* (n = 12).

Data shown are means ± SD. Statistical analysis was performed by two-tailed Mann-Whitney test in A-D.

Fig. 2

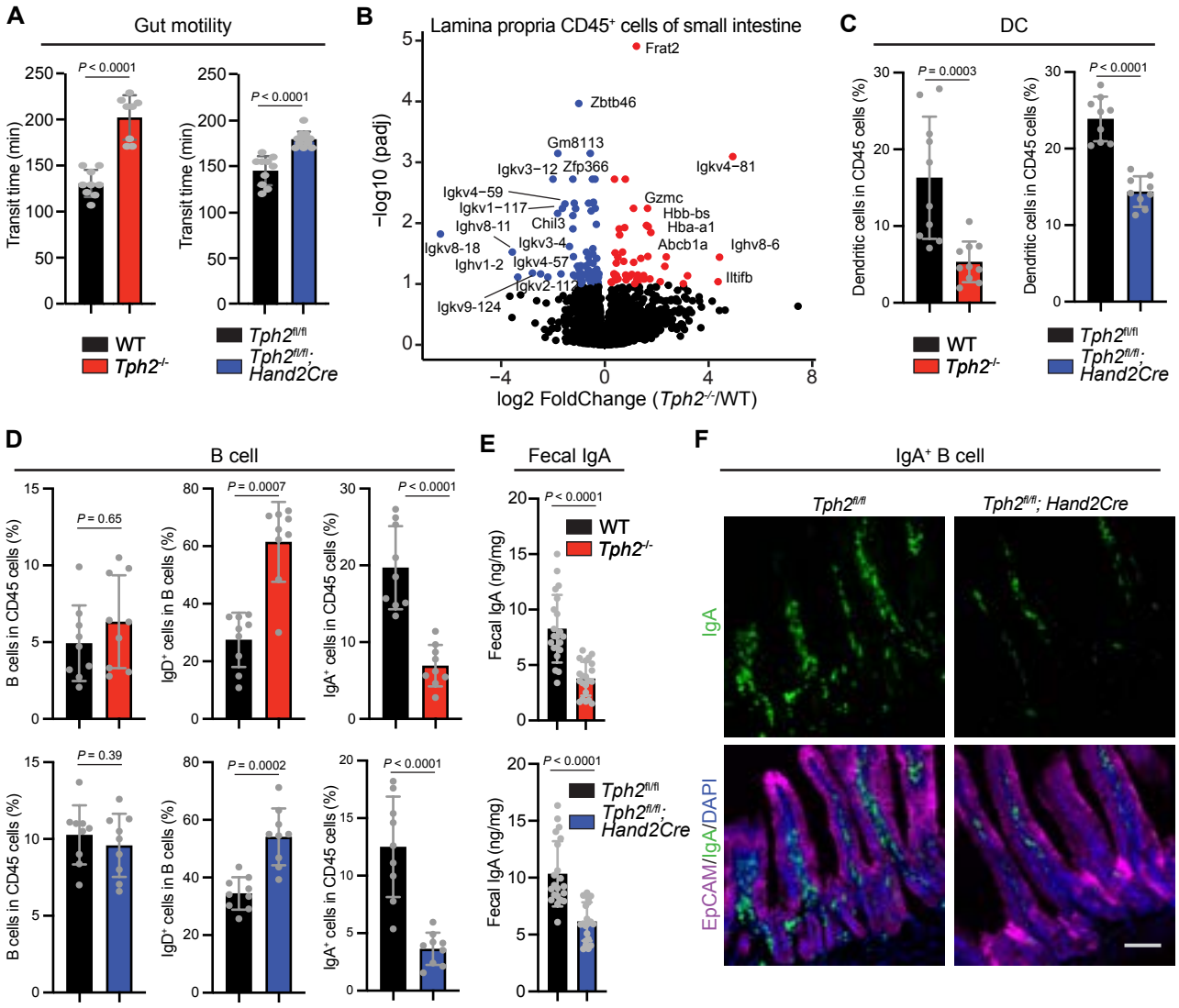

Figure 3. PSN control gut motility and the abundance of intestinal dendritic and IgA B cells.

(A) Total GI transit time was measured using carmine red assay in WT (n = 9) and *Tph2*$^{-/-}$ (n = 8) as well as *Tph2*$^{fl/fl}$ (n = 10) and *Tph2*$^{fl/fl}$*; Hand2-Cre* (n = 12) mice.

(B) Differential gene expression of CD45^{+} cells isolated from the lamina propria of the small intestine from co-housed WT and *Tph2*$^{-/-}$ mice. Red points indicate increased expression and blue points indicate decreased expression in *Tph2*$^{-/-}$ mice compared to WT mice.

(C, D) Flow cytometry analyses of frequency of DC (Live, CD45^{+}, MHC-II^{+}, CD64^{-}, CD11c^{+}) in lamina propria CD45^{+} cells from the small intestine of mice with the indicated genotypes (n = 9) (C), and the frequency of total B cells, IgD^{+} fraction of total B cells, and IgA^{+} cells in the lamina propria CD45^{+} cells from the small intestine of mice with indicated genotypes (n = 9) (D).

(E) Fecal IgA levels in mice with the indicated genotypes (n = 21 mice per group).

(F) Representative immunostaining of small intestine sections from mice of indicated genotypes. Epithelial cells are detected with EpCAM (magenta), IgA cells with anti-IgA antibody (green), and nuclei with DAPI (blue). Scale bar, 100 μm.

Data shown are means ± SD. Statistical analysis was performed by two-tailed Mann-Whitney test in A, and C-E.

Figure 3

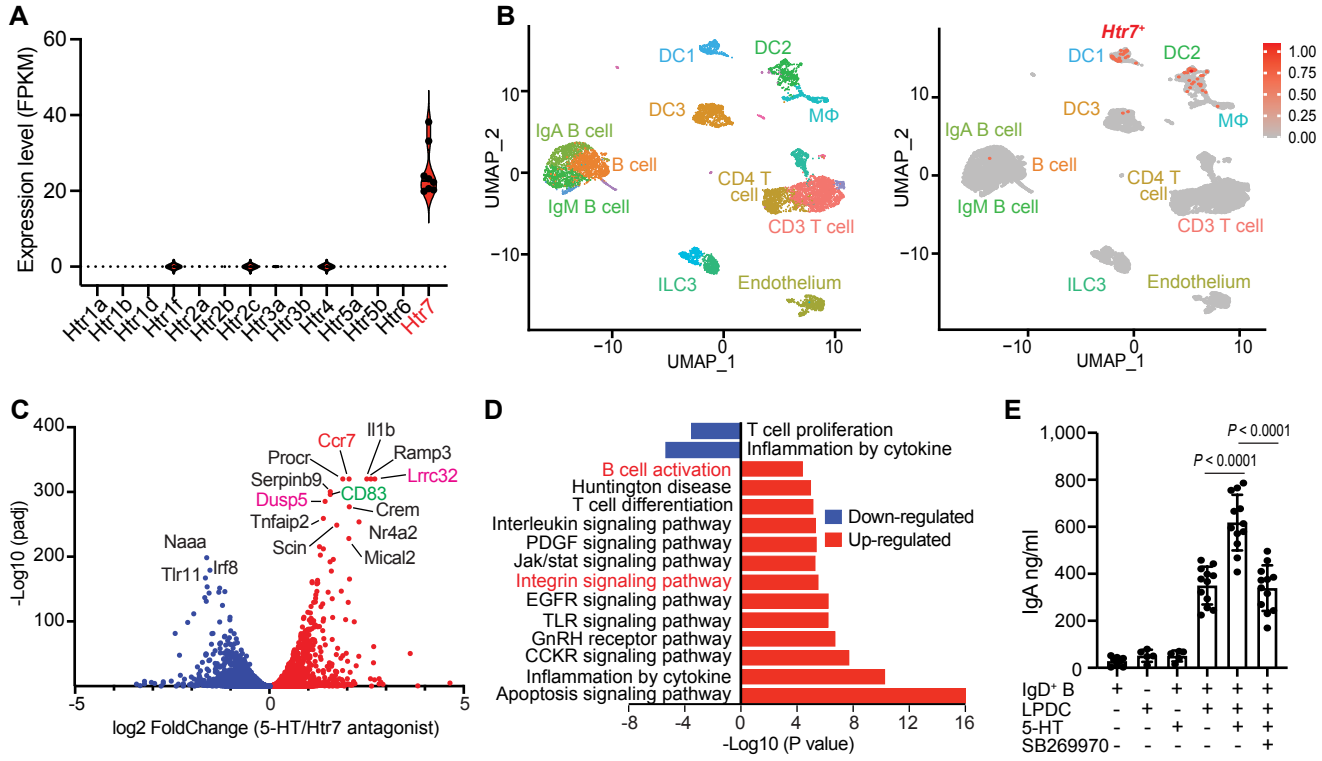

Figure 4. Serotonin remodels LPDC function to promote IgA⁺ B cell differentiation.

(A) Htr7 is the dominant serotonin receptor in LPDC. FPKM (Fragments Per Kilobase of transcript per Million fragments mapped) values of all serotonin receptors in LPDC.
(B) UMAP plot of single-cell transcriptome data (published in Xu et al.) of small intestinal lamina propria immune cells showing that expression of the Htr7 gene is restricted to LPDC cells.
(C) Differential gene expression in LPDCs treated with serotonin ±Htr7 antagonist. Red and blue points indicate genes whose expression was significantly increased or decreased respectively, in a Htr7-dependent fashion.
(D) GO pathways analysis of data from C.
(E) Tissue culture assay of IgA production from IgD⁺ B cells that were cocultured with LPDC, serotonin, and a Htr7 antagonist (SB269970) as indicated. The levels of IgA in the supernatants were measured by ELISA after 6 days of culture (n = 12). Data are representative of three independent experiments.
Data shown are means ± SD. Statistical analysis was performed by two-tailed Mann-Whitney test in E.

Figure 4

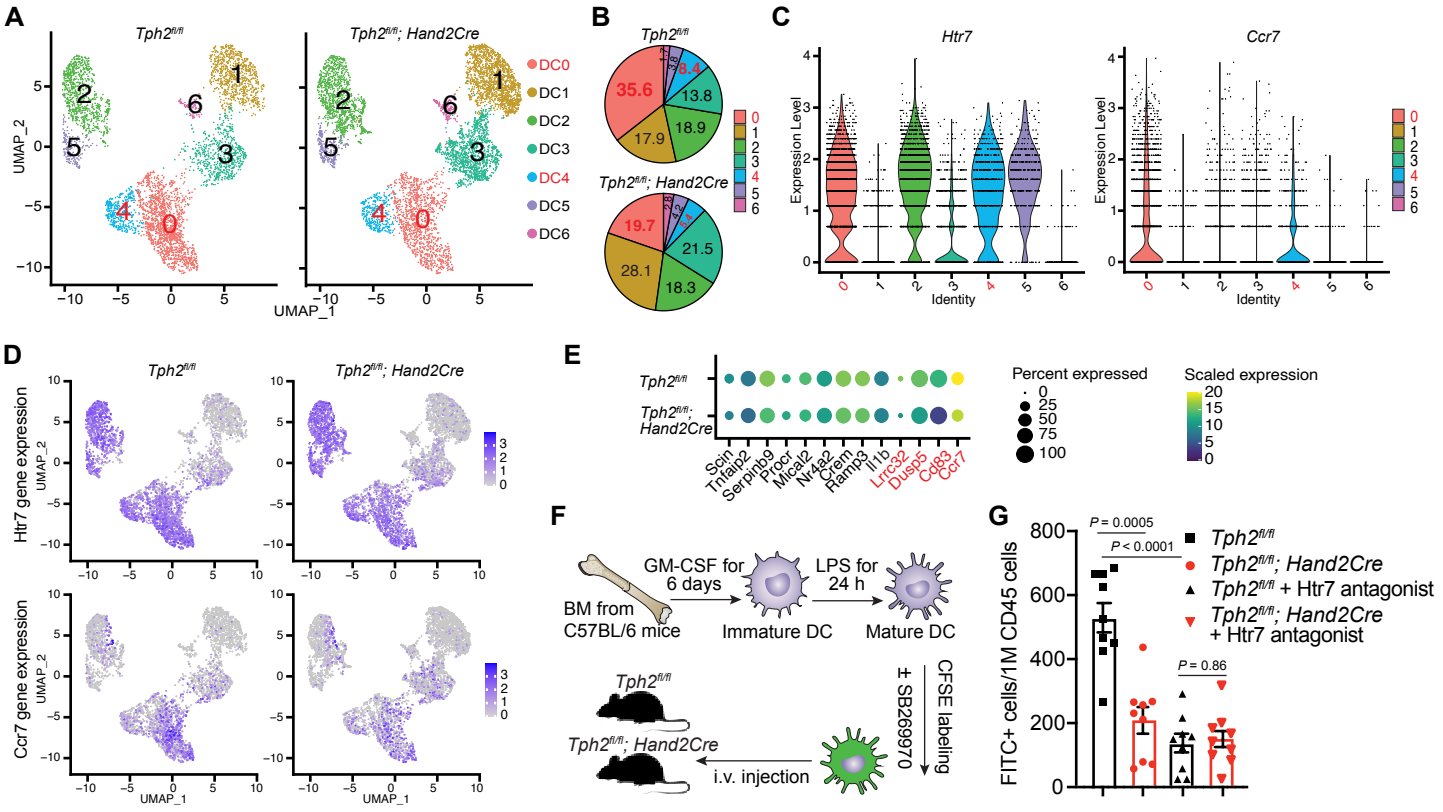

Figure 5. PSN remode LPDC function *in vivo*.

(A) UMAP plot of single-cell transcriptome data of small intestinal LPDCs from *Tph2*$^{fl/fl}$ and *Tph2*$^{fl/fl}$*; Hand2-Cre* mice.

(B) Pie charts showing the proportion of cluster 0 and 4 cells are decreased in *Tph2*$^{fl/fl}$ and *Tph2*$^{fl/fl}$*; Hand2-Cre* mice.

(C) Violin plots depicting the range of expression levels of *Htr7* and *Ccr7* in distinct LPDC clusters.

(D) UMAP plot derived from single-cell transcriptome data showing expression of *Htr7* and *Ccr7* in LPDCs from *Tph2*$^{fl/fl}$ and *Tph2*$^{fl/fl}$*; Hand2-Cre* mice. The color scale represents relative expression level.

(E) Comparison of the expression of the indicated genes in cluster 0 of LPDC between *Tph2*$^{fl/fl}$ and *Tph2*$^{fl/fl}$*; Hand2-Cre* mice. Dot color reflects the level of gene expression and dot size represents the percentage of cells expressing the indicated gene. The genes labeled in red are decreased in cluster 0 of LPDC in *Tph2*$^{fl/fl}$*; Hand2-Cre* mice and are consistent with the serotonin-induced genes observed *in vitro*.

(F) Schematic of the system used to analyze BMDC homing to the gut in *Tph2*$^{fl/fl}$ and *Tph2*$^{fl/fl}$*; Hand2-Cre* mice. Equal numbers of CFSE-labeled mature BMDCs were transplanted into *Tph2*$^{fl/fl}$ and *Tph2*$^{fl/fl}$*; Hand2-Cre* mice, and the CFSE^{+} cells in different tissues was analyzed 18 h post-transplantation.

(G) Frequency of CFSE^{+} cells among CD45^{+} cells in the lamina propria of *Tph2*$^{fl/fl}$ and *Tph2*$^{fl/fl}$*; Hand2-Cre* mice (n = 9).

Data shown are means ± SD. Statistical analysis was performed by two-tailed Mann-Whitney test in G.

Figure 5

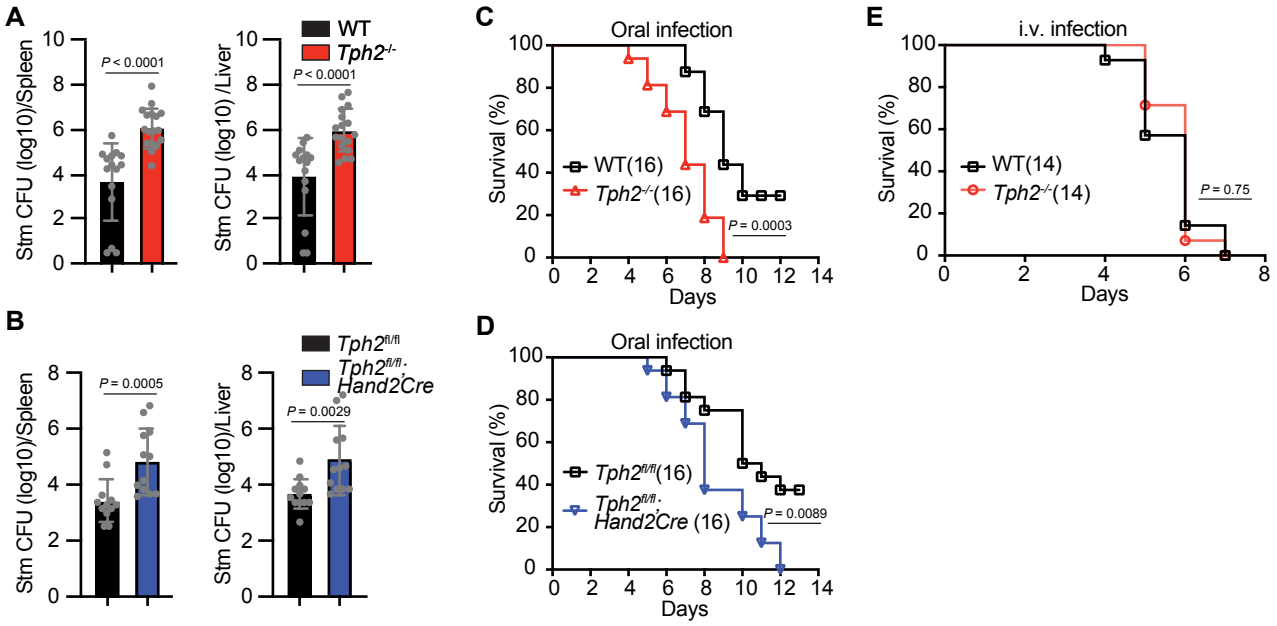

Figure 6. PSN boost host defense.

(A-B) Salmonella typhimurium (Stm) CFU burdens in livers and spleens of mice with the indicated genotypes (WT, n = 15; *Tph2*$^{-/-}$, n = 17; *Tph2*$^{fl/fl}$, n = 12; and *Tph2*$^{fl/fl}$*; Hand2-Cre*, n = 12) 5 days post oral inoculation.
(C-D) Kaplan Meier plot of survival of mice of indicated genotypes following oral *Salmonella* inoculation (n = 16).
(E) Kaplan Meier plot of survival of WT and *Tph2*$^{-/-}$ mice after intravenous *Salmonella* infection (n = 14).
Data shown are means ± SD. Statistical analysis was performed by two-tailed Mann-Whitney test in A, B; and by Log-rank test in C-E.

Figure 6

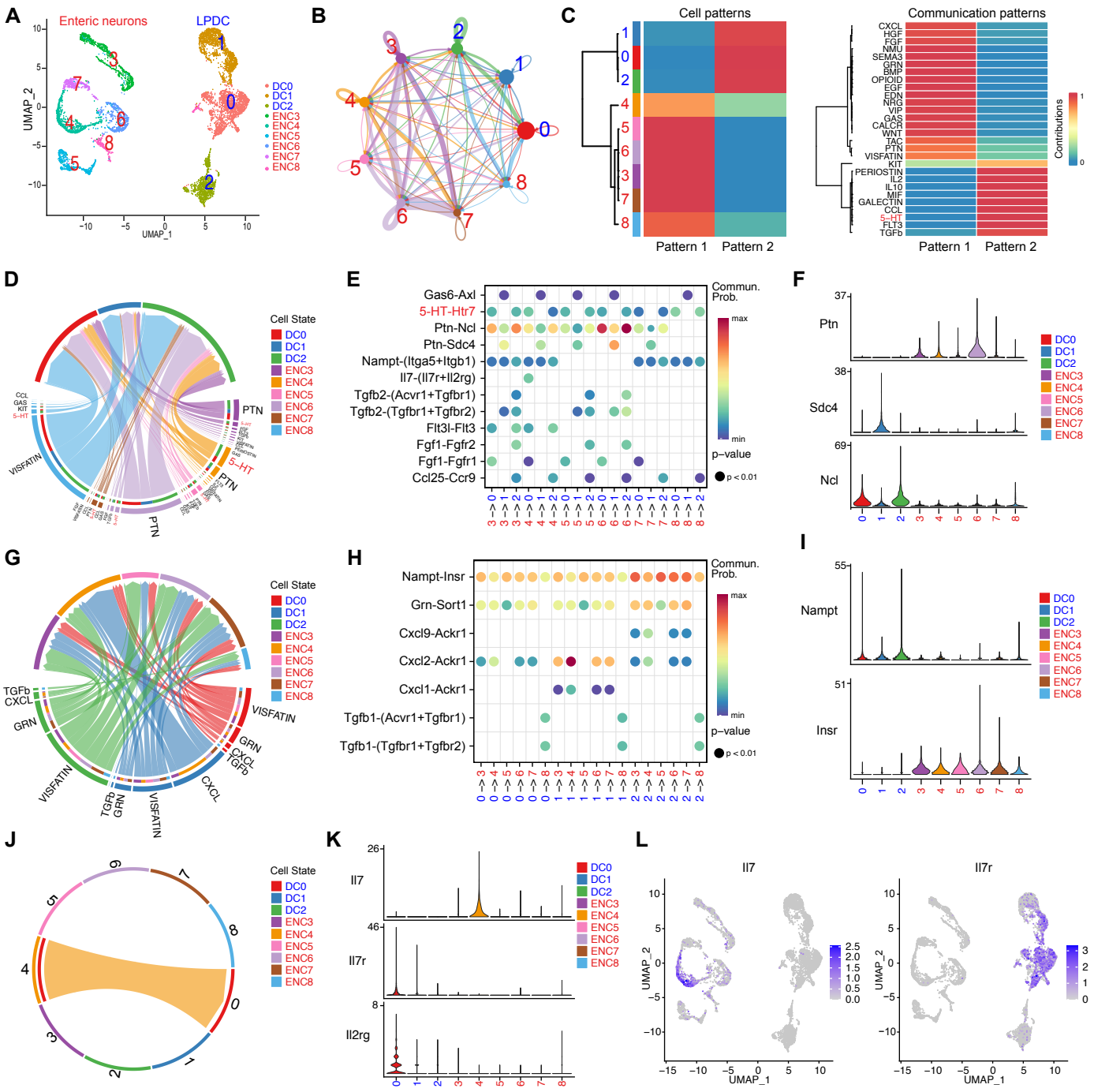
A
Enteric neurons
LPDC
UMAP_2
UMAP_1
DC0
DC1
DC2
ENC3
ENC4
ENC5
ENC6
ENC7
ENC8
B
C
Cell patterns
Communication patterns
Pattern 1
Pattern 2
Contributions
CXCL
HGF
FGF
NMU
SEMA3
GRN
BMP
OPIOID
EGF
EDN
NRG
VIP
GAS
CALCR
WNT
TAC
PTN
VISFATIN
KIT
PERIOSTIN
IL2
IL10
MIF
GALECTIN
CCL
5-HT
FLT3
TGFb
D
Cell State
PTN
5-HT
VISFATIN
E
Commun. Prob.
max
min
p–value
p < 0.01
Gas6-Axl
5-HT-Htr7
Ptn-Ncl
Ptn-Sdc4
Nampt-(Itga5+Itgb1)
Il7-(Il7r+Il2rg)
Tgfb2-(Acvr1+Tgfbr1)
Tgfb2-(Tgfbr1+Tgfbr2)
Flt3l-Flt3
Fgf1-Fgfr2
Fgf1-Fgfr1
Ccl25-Ccr9
F
Ptn
Sdc4
Ncl
G
TGFb
CXCL
GRN
VISFATIN
H
Nampt-Insr
Grn-Sort1
Cxcl9-Ackr1
Cxcl2-Ackr1
Cxcl1-Ackr1
Tgfb1-(Acvr1+Tgfbr1)
Tgfb1-(Tgfbr1+Tgfbr2)
I
Nampt
Insr
J
K
Il7
Il7r
Il2rg
L
Il7
Il7r
UMAP_2
UMAP_1

Figure 7

Figure 7. Bidirectional communication between enteric neurons and LPDCs.

(A) UMAP plot of single-cell transcriptome data of enteric neurons and lamina propria dendritic cells generated in this study that was used for analyzing cell-cell communication with CellChat.
(B) Circle network diagram of significant cell-cell interaction pathways. Arrows and line color indicate direction (ligand: receptor) and line thickness indicates the strength of the predicted interaction. The round loops represent the interactions within the same cell type.
(C) Heatmap showing the two global communication patterns calculated by the key signals for subpopulations between enteric neurons and LPDC cells.
(D-F) Enteric neuron to LPDC communication pathways. (D) Chord diagram showing all the significant interactions from enteric neuron to LPDC. (E) Dot plot showing the key ligand-receptor interactions in inferred communication pathways between subsets of enteric neurons and LPDC. Empty spaces indicate that the communication probability is zero. p-values were computed with a one-sided permutation test. The color scale represents communication probability as calculated in CellChat. (F) Violin plots illustrating the gene expression levels of the Ptn signaling pathway, with ligand expression in enteric neuron clusters and receptor expression in LPDC clusters.
(G-I) LPDC to enteric neuron communication pathway. (G) Chord diagram showing all the significant interactions from LPDC to enteric neuron. (H) Dot plot showing the key ligand-receptor interactions in inferred communication pathways between subsets of LPDC and enteric neurons. Empty spaces indicate that the communication probability is zero. p-values were computed with a one-sided permutation test. The color scale represents communication probability as calculated in CellChat. (I) Violin plots illustrating the gene expression levels of the Nampt-Insr signaling pathway, with ligand expression in LPDC clusters and receptor expression in enteric neuron clusters.
(J) Chord diagram displaying the communication network between enteric neuron cluster 4 and LPDC cluster 0, highlighting the targeting of Il7 from the former cell population to the Il7r located on the latter cell population.
(K) Violin plots illustrating the gene expression levels in distinct cell subtypes. Violin plot illustrating the gene expression levels of the of the IL7 signaling pathway, with ligand expression in enteric neuron cluster 4 and receptor (a heterodimer of Il7r and Il2rg) expression in LPDC cluster 0.
(L) UMAP plot derived from single-cell transcriptome data showing expression of Il7 in enteric neuron cluster 4 and Il7 receptor in LPDC cluster 0.

Figure 7